

Quantum simulation with hybrid tensor networks

Xiao Yuan,^{1,*} Jinzhao Sun,^{2,†} Junyu Liu,^{3,4,‡} Qi Zhao,^{5,§} and You Zhou^{6,¶}

¹*Stanford Institute for Theoretical Physics, Stanford University, Stanford California 94305, USA*

²*Clarendon Laboratory, University of Oxford, Parks Road, Oxford OX1 3PU, United Kingdom*

³*Walter Burke Institute for Theoretical Physics, California Institute of Technology, Pasadena, California 91125, USA*

⁴*Institute for Quantum Information and Matter,*

California Institute of Technology, Pasadena, CA 91125, USA

⁵*Joint Center for Quantum Information and Computer Science,*

University of Maryland, College Park, Maryland 20742, USA

⁶*Department of Physics, Harvard University, Cambridge, Massachusetts 02138, USA*

(Dated: July 3, 2020)

Tensor network theory and quantum simulation are respectively the key classical and quantum methods in understanding many-body quantum physics. Here we show hybridization of these two seemingly independent methods, inheriting both their distinct advantageous features of efficient representations of many-body wave functions. We introduce the framework of hybrid tensor networks with building blocks consisting of measurable quantum states and classically contractable tensors. As an example, we demonstrate efficient quantum simulation with hybrid tree tensor networks that use quantum hardware whose size is significantly smaller than the one of the target system. We numerically test our method for finding the ground state of 1D and 2D spin systems of up to 8×8 and 4×3 qubits with operations only acting on $8 + 1$ and $4 + 1$ qubits, respectively. Our approach paves the way to the near-term quantum simulation of large practical problems with intermediate size quantum hardware, with potential applications in quantum chemistry, quantum many-body physics, quantum field theory, and quantum gravity thought experiments.

I. INTRODUCTION

The major challenge in studying many-body quantum systems stems from the hardness of efficient representation of the wave function, whose dimension in principle scales exponentially to the system size. Among all modern classical approaches, the tensor network theory originated from the density matrix renormalization group for 1D Hamiltonians [1, 2], has now become one of the key methods in understanding both static and dynamic properties of many-body quantum physics [3]. The tensor network theory relies on an efficient classical description or compression of many-body entanglement with a network consisting of low-rank tensors. Despite its notable success in various problems, the tensor network theory may become inadequate for general strongly interacting systems that do not admit an efficient tensor network description.

This motivates an alternative approach of quantum simulation, as initially proposed by Feynman, which uses controlled quantum hardware to represent the target quantum system naturally [4]. A quantum computer can efficiently represent complex many-body entanglement and may solve strongly interacting systems, such as quantum chemistry problems or the 2D Hubbard model [5, 6]. Although, realizing universal quantum

computers remains a major challenge to current technology [7]. A more realistic scenario is to consider the noisy intermediate-scale quantum (NISQ) era, where we apply a shallow circuit on a limited number of noisy qubits [8]. However, the power of NISQ devices is limited, and they may become incapable of solving problems requiring large numbers of qubits or deep circuits.

Here we study a hybrid approach that combines tensor network theory and quantum simulation. We introduce a framework of the hybrid tensor network consisting of classical low-rank tensors and many-body quantum states. By leveraging the ability of tensor networks in the efficient classical representation of quantum states, we thus extend the power of NISQ devices in describing large complex quantum systems with a small quantum processor. Similar task-specific schemes have been studied for hybrid chemistry computation that goes beyond the active-space approximation without extra quantum resources [9], and for 1D systems via the concatenation of quantum states to a matrix product state [10]. Our result, on the one hand, gives a unified framework for these existing task tailored schemes; Yet, more importantly, it provides the basis for general hybrid classical-quantum representation of many-body wave functions that may be applicable to general problems.

While the mathematical definition of the hybrid tensor network is consistent with that of conventional tensor network theories, tensor contractions are operationally realized in different ways depending on whether the tensor is a classical tensor or a quantum state. By showing how to obtain expectation values of local observables, we apply the hybrid tensor network in studying static and dynamic problems of quantum systems [11, 12]. With the

* xiao.yuan.ph@gmail.com

† jinzhao.sun@physics.ox.ac.uk

‡ jliu2@caltech.edu

§ zhaoq@umd.edu

¶ you.zhou@g.harvard.edu

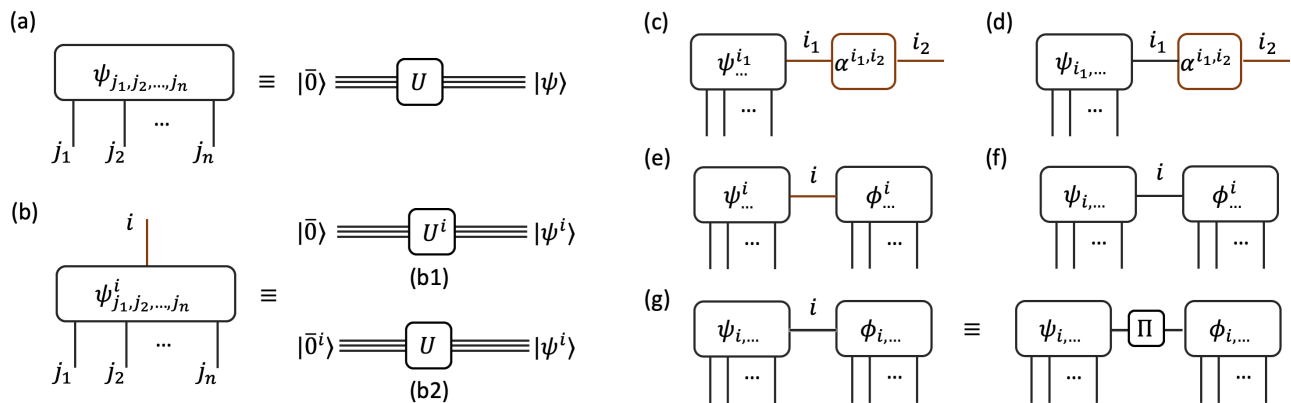


FIG. 1. Tensor network representation of quantum states and tensor contractions. (a) A general n -partite quantum state can be regarded as a rank- n tensor. (b) We add a classical index to an n -partite quantum state to generate a rank- $(n+1)$ tensor with n indices representing n quantum systems and 1 classical index. With a quantum circuit, it is equivalent to preparing different states $|\psi^i\rangle = U^i |i\rangle$ with (b1) different unitary operations as $|\psi^i\rangle = U^i |\bar{0}\rangle$ or (b2) simply the same unitary but different initial states as $|\psi^i\rangle = U |\bar{0}^i\rangle$. (c, d) Tensor contractions between a quantum tensor and a classical tensor. (e, f, g) Tensor contractions between two quantum tensors. (c, e) The contracted index of both tensors corresponds to a classical index. (d, f) The contracted index corresponds to a classical index for one tensor and a quantum index for another tensor. (g) The contracted index of both tensors corresponds to a quantum index. The tensor Π is equivalent to a projective measurement $\sum_{i=i'} |i\rangle \langle i| \otimes |i'\rangle \langle i'|$.

example of hybrid tree tensor networks, we show how to use a small quantum processor for efficiently representing large quantum systems. We numerically test our method by finding ground states of a 1D spin cluster with up to 8×8 qubits and a 2D spin web with up to 4×3 qubits, with quantum processors on $8+1$ qubits and $4+1$ qubits, respectively. We discuss the application of our result in chemistry, condensed matter physics, quantum field theory, and quantum gravity, and conclude the outlook for near-term quantum simulations.

II. HYBRID TENSOR NETWORK

A. Framework

We first introduce the basic framework of the hybrid tensor network. We focus on qubits, and the results can be straightforwardly generalized to higher dimensions. A rank- n tensor, when regarded as a multi-dimension array, can be represented as T_{j_1, j_2, \dots, j_n} with n indices. The amplitude of an n -partite quantum state can be interpreted as a rank- n tensor in the computational basis,

$$|\psi\rangle = \sum_{j_1, j_2, \dots, j_n} \psi_{j_1, j_2, \dots, j_n} |j_1\rangle |j_2\rangle \dots |j_n\rangle, \quad (1)$$

which has degrees of freedom that are exponential to n . A classical tensor network consists of low-rank tensors, and it can efficiently describe physical states that lie in a small subset of the whole Hilbert space. For example, a matrix product state (MPS) [13] is defined by

$$|\psi\rangle = \sum_{j_1 \dots j_n} \text{Tr}[A^{j_1} \dots A^{j_n}] |j_1 \dots j_n\rangle, \quad (2)$$

and it consists of rank-3 tensors with the dimension of each matrix A^{j_k} , i.e., the bond dimension χ , being a small number. Suppose the state is an n -qubit state, the MPS representation thus compresses the dimension from $O(2^n)$ to $O(n\chi^2)$.

Contrary to a classical network, a quantum state $|\psi\rangle$ can be naturally represented with a quantum computer by applying a unitary circuit U to an n -qubit initial state $|\bar{0}\rangle$ as $|\psi\rangle = U |\bar{0}\rangle$. The circuit generally consists of a sequence of parameterized single and two-qubit gates, which can be adjusted to produce different output states. As shown in Fig. 1(a), we regard the quantum state $|\psi\rangle$ as a rank- n tensor. With the state shown in Eq. (1), the n indices correspond to the computational basis of each system. In addition, we can add a classical index i to the n -qubit state to form a rank- $(n+1)$ tensor. As shown in Fig. 1(b), suppose the dimension of the classical index is χ , the rank- $(n+1)$ tensor represents χ numbers of quantum states $\{|\psi^i\rangle\}$. These states can be obtained from applying different circuits U_i to the same initial state as $|\psi^i\rangle = U^i |\bar{0}\rangle$, or simply the same unitary U to different initial states as $|\psi^i\rangle = U |\bar{0}^i\rangle$.

In this work, we regard low-rank tensors as classical tensors and quantum states as quantum tensors. We define a hybrid tensor network as a network constructed by connecting both classical and quantum tensors. To distinguish quantum and classical tensors, we put indices corresponding to classical labels and quantum bases to the superscript and subscript of the tensor, respectively. For example, the tensor A^{i_1, i_2} represents a classical tensor with two classical indices and $\psi_{j_1, j_2, \dots, j_n}^i$ represents a set of quantum states with one classical index and n bases. Two tensors, being either classical or quantum, are connected by following the conventional contraction

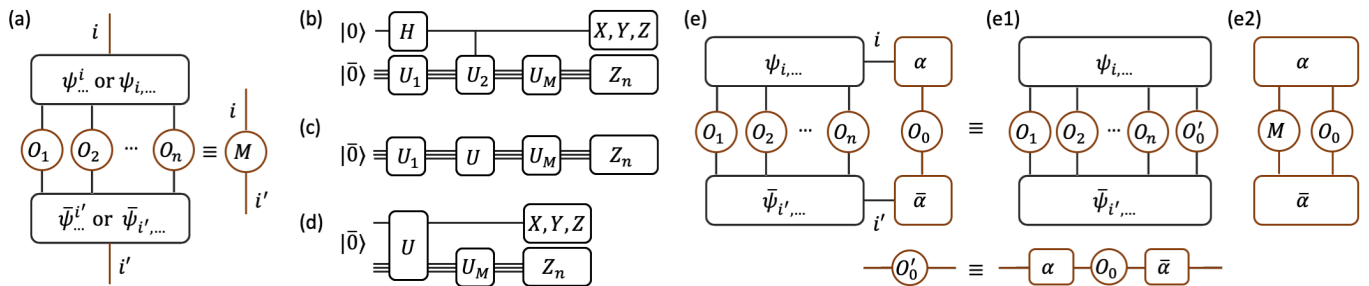


FIG. 2. Measuring expectation values of a quantum tensor. (a) Consider a rank-($n+1$) quantum tensor, which could be either an n -partite quantum state with a classical index i or an $(n+1)$ -partite quantum state with a quantum basis index i . The expectation value of the n quantum systems gives a hermitian observable $M^{i',i} = \langle \psi^{i'} | O_1 \otimes O_2 \otimes \dots \otimes O_n | \psi^i \rangle$ on the open indices. Each element $M^{i',i}$ can be measured with a quantum circuit of (b), (c), or (d). (b) Suppose the index i is classical and $|\psi^i\rangle = U^i |\bar{0}\rangle$, we choose $U_1 = U^i$, $U_2 = U^{i'} (U^i)^\dagger$, and U_M to be the unitary that rotates the eigenstates of the observables to the computational basis. We get each $M^{i',i}$ by measuring the ancillary qubit in the X, Y, Z bases and the other n qubits in the computational Z basis. (c) Suppose the index i is classical and $|\psi^i\rangle = U |\bar{0}^i\rangle$, we use U_1 to prepare four input states $|\bar{0}^i\rangle, |\bar{0}^{i'}\rangle, (|\bar{0}^i\rangle + |\bar{0}^{i'}\rangle)/\sqrt{2}, (|\bar{0}^i\rangle - |\bar{0}^{i'}\rangle)/\sqrt{2}$ and each $M^{i',i}$ corresponds to a linear combination of the measurement results. (d) Suppose the index i is quantum, after applying the unitary U for preparing the state $|\psi\rangle = U |\bar{0}\rangle$, we measure n qubits in the computational basis and the qubit with index i in the Pauli X, Y , and Z bases. (e) Tensor contraction can have different orders. With a rank-($n+1$) quantum tensor connected to a classical tensor, we can either (e1) first calculate the expectation value of the classical tensor and then measure the $(n+1)$ -partite quantum state or (e2) first measure the n systems via (d) and then do classical tensor contraction.

rule of tensor networks, such as $C^{i_1, i_3} = \sum_{i_2} A^{i_1, i_2} B^{i_2, i_3}$.

Depending on whether the tensor and the contracted index is classical or quantum, we list the five cases in Fig. 1(c)-(g). For example, in Fig. 1(c), we contract the classical index i_1 between a quantum tensor $\psi^{i_1, \dots}$ and a classical tensor α^{i_1, i_2} , producing a new tensor $\bar{\psi}^{i_2} = \sum_{i_1} \alpha^{i_1, i_2} \psi^{i_1, \dots}$. Here we use \dots as a short for the subscripts of a quantum tensor. When the contracted index corresponds to a quantum basis of $\psi_{i_1, \dots}$, its contraction with α^{i_1, i_2} is similarly defined as $\bar{\psi}^{i_2} = \sum_{i_1} \alpha^{i_1, i_2} \psi_{i_1, \dots}$. Even though the contraction rules between Fig. 1(c) and (d) are mathematically similar, they correspond to different cases when considering the contraction of the remaining indices. The major difference originates from different ways of contracting the indices of quantum and classical tensors. As we shortly discuss, when calculating expectation values of local observables, the indices of quantum tensors are contracted via a measurement on the quantum state, whereas indices of classical tensors are always contracted via matrix multiplication. Therefore, when connecting a quantum index and a classical index, whether the index is contracted via a measurement or matrix multiplication will lead to a difference.

Similarly, when connecting two quantum tensors, there are three cases with the two contracted indices having 0, 1, and 2 quantum indices, as shown in Fig. 1(e), (f), and (g), respectively. The cases of (e) and (f) are similar to (c) and (d). Case (g) can be equivalently understood as applying a projective measurement $\Pi = \sum_{i=i'} |i\rangle \langle i| \otimes |i'\rangle \langle i'|$ on the connected two qubits. Since the measurement probability could be less than 1, the probability for connecting r times of two quantum indices decays exponentially with r . We can thus only

have a constant number r of contraction between two quantum indices. We also refer to the Appendix for a quantum state interpretation of these five cases.

B. Calculating expectation values of local observables

Next, we show how to calculate the expectation values of local observables on a hybrid tensor network state. We first show the basic rules for simple classical and quantum tensors. For classical tensors, the expectation value is calculated in the same way as tensor contraction. For quantum tensors, the expectation value is obtained by measuring the quantum state. As shown in Fig. 2(a), we consider the expectation values on the n systems of a rank-($n+1$) quantum tensor. By measuring the n systems, it gives a new rank-2 tensor $M^{i',i}$ with two open indices i and i' . When the open indices are classical, we can measure each element $M^{i',i}$ via quantum circuits in Fig. 2(b) or (c) depending on how the tensor is defined. When the open indices correspond to bases of quantum states, we measure $M^{i',i}$ via Fig. 2(d). In particular, we need to measure the expectation values of the contracted n systems and the system with open indices in the three Pauli bases. We refer to the Appendix for details.

When calculating the expectation values of a general hybrid tensor network, we can follow the basic rules for each tensor. However, similar to the case of conventional tensor networks, different orders of tensor contraction could lead to different complexities. We consider an example of a simple tensor network of Fig. 1(d) by connecting an $(n+1)$ -partite quantum state to a rank-2

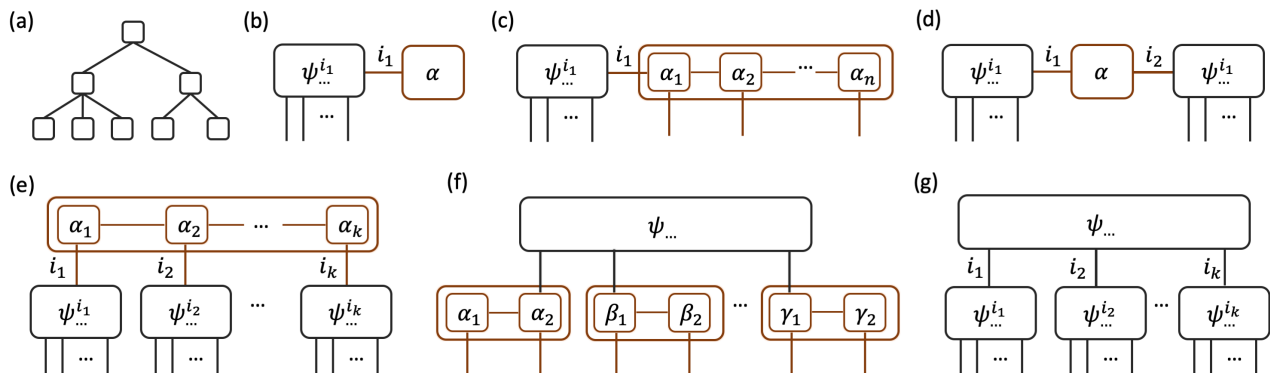


FIG. 3. Hybrid quantum-classical tensor network. (a) An example of tree structure. (b) We extend the power of the quantum tensor by adding a classical tensor. (c) We combine a quantum tensor and a classical tensor network to represent a state in a larger Hilbert space. (d) We use a classical tensor to connect two quantum tensors. (e) Generalization of (d) with multiple subsystems. (f) We use classical tensors to represent local correlation and a quantum tensor to represent correlations between subsystems. (g) A quantum-quantum network. The indices connecting the first and the second layers are quantum for nodes from the first layer and classical for nodes from the second layer.

classical tensor. We consider the expectation value of the $(n+1)$ -partite quantum state of the network, as shown in Fig. 2(e). It can be obtained by either firstly contracting the classical tensor and then measure the $(n+1)$ -partite quantum state as in Fig. 2(e1); or firstly measuring the n -partite state and then contract the classical tensor as in Fig. 2(e2). Suppose we neglect the classical computation cost, Fig. 2(e1) only requires a single measurement (with \mathcal{M} repeated samples) on the quantum state, whereas Fig. 2(e2) needs three measurements (with $3\mathcal{M}$ samples). For a general hybrid tensor network, we thus also need to optimize the order of tensor contraction.

III. HYBRID TREE TENSOR NETWORK

Similar to the case of conventional tensor networks, the contraction of a general-structured hybrid tensor network may have complexity that is exponential to the system size. It explains why existing tensor network theories focus on tensor networks with specific structures, including 1D matrix product states (MPS) [14–16], 2D projected entangled pair states (PEPS) [17], tree tensor networks (TTN) [18], multiscale entanglement renormalization ansatz (MERA) [19], etc. Here we consider hybrid tensor networks with a tree structure, as shown in Fig. 3(a), which generally admits an efficient tensor contraction. The basic idea is to use either a quantum tensor or a classical tensor as nodes that form a tree structure. The classical tensor can be either a low-rank tensor or any efficiently contractable classical tensor network. Quantum tensors are tensors of quantum states possibly associated with a constant number of classical indices.

We give several examples of hybrid TTN in Fig. 3 with trees whose depth is at most two. With a simple tree, we can connect a classical tensor to a quantum tensor, so that it either extends the state subspace, as in Fig. 3(b),

or represents virtual qubits as in Fig. 3(c). In particular, denoting the classical tensor to be α^i , the network in Fig. 3(b) describes a subspace $\{|\psi\rangle = \sum_i \alpha^i |\psi^i\rangle\}$, which, when applied in quantum simulation, is a generalization of the subspace expansion method that has been widely used for several tasks, including finding excited energy spectra [20], error mitigation [21], and error correction [22]. In Fig. 3(c), the classical tensor is further used to represent virtual qubits beyond the ones represented by the quantum state. This corresponds to the scenario where the quantum state is only used to represent the active space of the problem, whose other virtual space is approximated by a classical tensor as in quantum chemistry simulation [9]. The tensor network in Fig. 3(d) describes two subsystems, with each one represented by a quantum state and their weak interaction represented by a classical tensor, corresponding to a similar scenario considered in Ref. [10]. Its generalization to multiple subsystems is given in Fig. 3(e), where entanglements of local subsystems are described by quantum states, and the correlation between local subsystems is described classically. Such a hybrid tensor network may be useful for describing weakly coupled subsystems, such as the correlation between electrons and nucleus of molecules beyond the Born-Oppenheimer approximation [23]. We can also use classical tensors to represent local correlations and a quantum tensor to represent the non-local correlation, as shown in Fig. 3(f). Here we use a small classical tensor to represent the local correlation, which can be understood as an effective renormalization procedure. When a large classical tensor network is used for the local subsystem, it may also be useful for studying topological order with long-range entanglement [24, 25]. Note that we use the MPS as the example, and other classical tensor networks such as MERA can be similarly used. In addition to representing either local correlations or non-local correlations with classical tensors, we can also represent both of them with quantum states, as shown in Fig. 3(g). Here

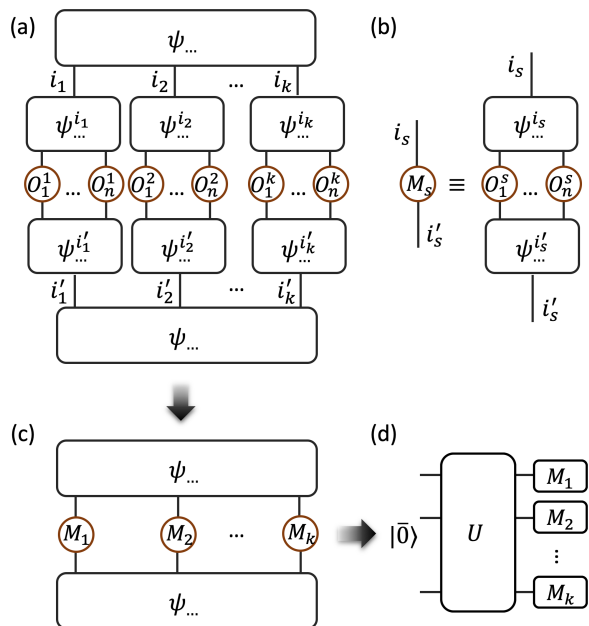


FIG. 4. An example for calculating expectation values of a hybrid TTN. Considering a hybrid TTN of Fig. 3(g), the expectation value of local observables $\otimes_{i=1}^k \otimes_{j=1}^n O_j^i$ corresponds to tensor contraction of (a). We first calculate the observable M^{i_s, i'_s} for each tensor on the second layer as (b) with quantum circuits shown in Fig. 2(b,c). Then tensor contraction of (a) reduces to the contraction of (c), which corresponds to a quantum circuit representation in (d) that prepares the state $|\psi\rangle$ with $|\psi\rangle = U|\bar{0}\rangle$ and measures the observables $M_1 \otimes \dots \otimes M_k$.

the contracted indices of the second layer quantum tensors are classical, and we show in Fig. 4 that expectation values of local observables can be efficiently obtained.

A general hybrid TTN can have an arbitrary tree structure, with each node being either a classical or quantum tensor. For a tree with maximal depth D and maximal degree g , the cost for measuring local observables of a hybrid TTN scales as $\mathcal{O}(g^{D-1})$. While the hybrid TTN represents a system of $N = \mathcal{O}(g^{D-1})$ qubits, the cost is also linear to the system size N . For the entanglement properties of hybrid TTN, it can represent entanglement beyond the area law with long-range correlation. We refer to the Appendix for details. Since the hybrid TTN represents a large set of quantum states and admits efficient calculation of local observables, it can be applied as the ansatz for variational quantum simulation algorithms for solving static and dynamic problems of many-body quantum systems.

IV. NUMERICAL SIMULATION

Now we numerically test variational quantum simulation with hybrid tensor networks. We consider finding ground states of the 1D spin cluster and 2D spin web systems with nearest-neighbor interactions and external

fields, as shown in Fig. 5(a). For the 1D spin cluster, we regard each adjacent $n = 8$ qubits as a subsystem and consider $k = 2, 3, \dots, 8$ subsystems with $n \times k$ qubits. The total Hamiltonian is

$$H = \sum_{j=1}^k H_j + \lambda H_{\text{int}}, \quad (3)$$

where the Hamiltonian H_j of the j th subsystem and the interaction H_{int} between the subsystems are

$$H_j = \sum_{i=1}^7 f \hat{Z}_{8j+i} \hat{Z}_{8j+i+1} + \sum_{i=1}^8 \left(g \hat{X}_{8j+i} + h \hat{Z}_{8j+i} \right),$$

$$H_{\text{int}} = \sum_{j=1}^{k-1} f_j \hat{Z}_{8j} \hat{Z}_{8j+1},$$

with X_i and Z_i being Pauli operators acting on the i th qubit, and λ being a parameter for tuning the interaction strength. We also consider a system of spins on a 2D $n \times k$ web with $n = 4$ and $k = 3$. We group each 4 qubits in the same row as a subsystem and the total Hamiltonian is represented as Eq. (3) with

$$H_j = \sum_{i=1}^3 f \hat{Z}_{j,i} \hat{Z}_{j,i+1} + \sum_{i=1}^8 \left(g \hat{X}_{j,i} + h \hat{Z}_{j,i} \right),$$

$$H_{\text{int}} = \sum_{j=1}^{k-1} \sum_{i=1}^4 f_{j,i} \hat{Z}_{j,i} \hat{Z}_{j+1,i}$$

where $X_{j,i}$ and $Z_{j,i}$ are Pauli operators acting on site (j, i) . In the simulation, we assume that interactions in each subsystem are identical with $f = 1$, while interactions between subsystems $\{f_j\}$ or $\{f_{j,i}\}$ are generated randomly from $[0, 1]$. The parameters of the external fields are set to be $h = 0.318$ and $g = 0.5$. The Hamiltonians are similar to some toy models representing certain features of holographic bulk in the $2 + 1$ dimension [26], and we refer to the Appendix for further discussions. Moreover, the model captures some properties of charged black holes. For instance, the Penrose diagram of the Reissner-Nordström or the Kerr black hole in four dimensions is a chain of black or white holes, old or new universes, while quantum information might be propagating among different patches of the spacetime (see, for instance, [27]).

Here, we use the hybrid TTN of Fig. 3(g) to be the ansatz and variationally change the parameters to approximate the ground state. For the hybrid TTN in Fig. 3(g), suppose the quantum state of the first layer is generated as $|\psi\rangle = V(\vec{\theta}_0)|\bar{0}\rangle = \sum \alpha_{i_1, \dots, i_k} |i_1, \dots, i_k\rangle$ and the quantum states of the j th subsystem of the second layer are $|\psi_j^{i_j}(\vec{\theta}_j)\rangle = U(\vec{\theta}_j)|\bar{0}^{i_j}\rangle$. The circuits of V and U are the hardware efficient ansätze, as shown in Fig. 5(b) with initial states $|\bar{0}^{i_j}\rangle = |i_j\rangle^{\otimes n}$ with $i_j \in \{0, 1\}$ and the number of qubits of the subsystem n . The hybrid

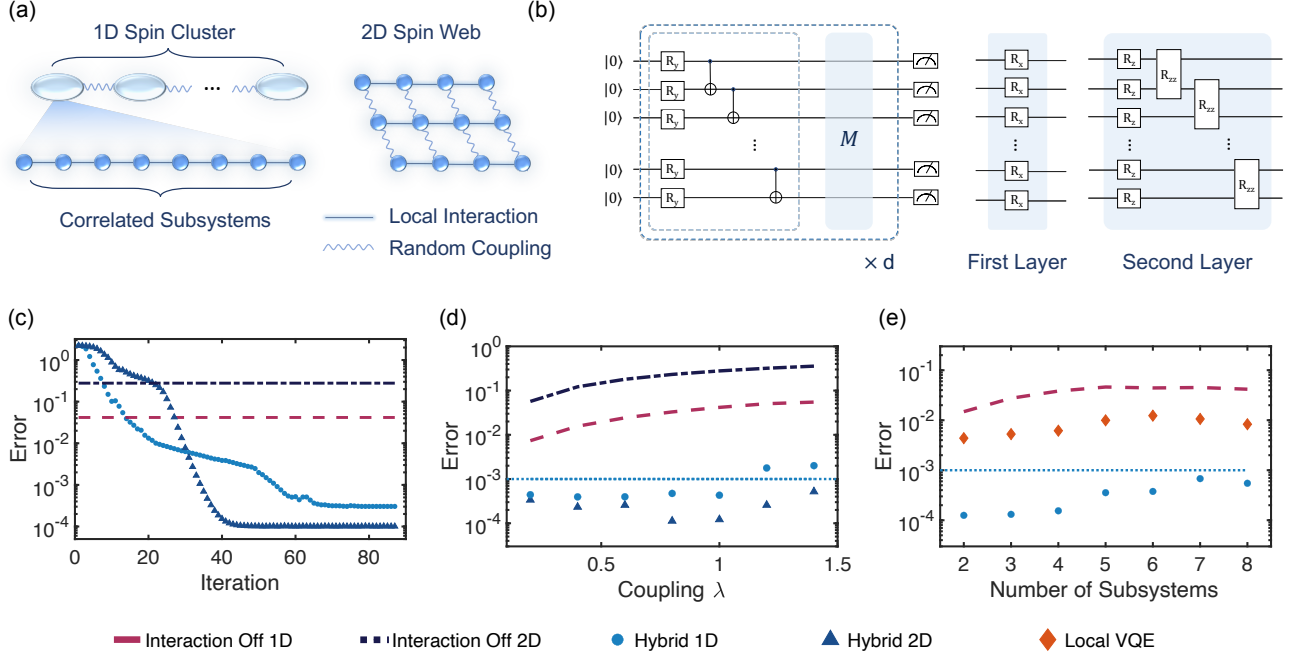


FIG. 5. Numerical set-up and simulation results for 1D and 2D correlated quantum systems with hybrid TTN. (a) Sketch for the 1D spin cluster and 2D spin web with nearest-neighbor correlations. We group 8 adjacent qubits and 4 horizontal qubits as subsystems for the 1D and 2D systems, respectively. The couplings of particles in each subsystem are identical with $f = 1$, and the couplings between subsystems are generated randomly from $[0, 1]$ multiplied by a tunable parameter λ . (b) The ansatz circuit for the quantum tensors in Fig. 3(g). The circuits share similar structures with d repetitions of the circuits in the dashed box. Here, R_α ($\alpha \in \{X, Y, Z\}$) represents single qubit rotation around the α axis and the two qubit gate is $R_{ZZ}(\theta_i) = e^{-i\theta_i Z \otimes Z}$. The rotation angle (parameter) for each gate is initialized from a small random value and updated in each variational cycle. In the simulation, the circuit depths for V (first layer tensor) and U (second layer tensor) are set to be $d(U) = 8$, $d(V) = 4$. The additional unitary M is inserted at the 1st and $[d/2 + 1]$ th block. (c)-(f) shows the numerical simulation result of the ground state energy E of the 1D and 2D quantum systems. For the 1D case, we compare E to the reference result $E_0 = E_{\text{MPS}}$ obtained from a standard DMRG implementation with a bond dimension $\chi = 32$; For the 2D case, we compare E with exact diagonalization $E_0 = E_{\text{Exact}}$. We use the relative error $1 - E/E_0$ to characterize the calculation accuracy. The red dashed line (for 1D) and blue dash-dotted line (for 2D) correspond to the ground state energy with no interaction between subsystems, i.e., $\lambda = 0$. The cyan dot (for 1D) and blue triangle (for 2D) are results obtained with hybrid tensor networks. The red diamond represents results via applying variational quantum eigensolver (VQE) locally on product states of subsystems. (c) We show the convergence towards the ground state for the 1D 8×8 and 2D 4×3 systems with $\lambda = 1$ by using imaginary time evolution optimization with adaptive time steps. (d) We compare the error of the results with respect to different subsystem coupling strength λ for the 1D 8×8 and 2D 4×3 systems. (e) For the 1D system with $8 \times k$ qubits, we show the calculation error with different numbers of local subsystems $k \in \{2, 3, \dots, 8\}$ with $\lambda = 1$.

TTN thus represents a quantum state as

$$|\tilde{\psi}(\vec{\theta})\rangle = \sum_{i_1 \dots i_k} \alpha_{i_1, \dots, i_k}(\vec{\theta}_0) |\psi_1^{i_1}(\vec{\theta}_1)\rangle \otimes \dots \otimes |\psi_k^{i_k}(\vec{\theta}_k)\rangle, \quad (4)$$

with $\vec{\theta} = (\vec{\theta}_0, \vec{\theta}_1, \dots, \vec{\theta}_k)$ representing all the parameters. Since we have $\langle \psi_j^{i'_j} | \psi_j^{i_j} \rangle = \delta_{i'_j, i_j}$, the state is automatically normalized. For parameters $\vec{\theta}$, we obtain the expectation value of the Hamiltonian $E(\vec{\theta}) = \langle \tilde{\psi}(\vec{\theta}) | H | \tilde{\psi}(\vec{\theta}) \rangle$ by following the contraction rule of Fig. 4. In particular, we first measure the observables of the second layer states and then measure the effective observables of the first layer state. To minimize the energy $E(\vec{\theta})$, the parameters are optimized by the variational imaginary time

evolution method [28]. We leave the details for the implementation of the variational imaginary time evolution method to the Appendix. We note that an extra ancillary qubit is required for variational imaginary time evolution. Therefore the quantum system needed for simulating the $8 \times k$ -qubit 1D and 4×3 -qubit 2D systems are $8 + 1$ and $4 + 1$ qubits, respectively.

We benchmark the calculation by comparing the results for 1D systems with ones obtained from open-boundary matrix product states (MPS), and the results for 2D systems with ones from exact matrix diagonalization. Suppose the ground state energy from hybrid TTN calculation is E , and the one from MPS or exact matrix diagonalization is E_0 , we show the relative calculation error $1 - E/E_0$ under different cases. In Fig. 5(c), we

consider the 1D spin cluster with 8×8 qubits and the 2D spin web with 4×3 qubits both with coupling strength $\lambda = 1$. We show the convergence of the ground state energy under the variational optimization method with the relative error below 10^{-3} . The calculation thus verifies the capability of efficient representation of the ground states with hybrid TTN.

Next, we study how the interaction strength or the number of subsystems affect the efficacy of the hybrid TTN. As shown in Fig. 5(d), we present the calculation error with respect to different coupling strength λ for the 8×8 -qubit 1D and 4×3 -qubit 2D systems. We can see that although the error fluctuates with different coupling strength, which might owe to instability from the optimization, the error remains consistent around 10^{-3} . In Fig. 5(e), we show the calculation error for the $8 \times k$ -qubit 1D cluster with different k subsystems. For coupling strength $\lambda = 1$, we observe a consistent error below 10^{-3} . These results with different coupling strength and different numbers of subsystems verify the robustness of the hybrid TTN method.

However, from the simulation results, we do observe the trend of larger errors with increasing interactions or more subsystems, aligning with the intuition that general strongly-coupled systems are hard to simulate. Indeed, we are not expecting the hybrid TTN applies universally to general quantum systems in a similar way to universal quantum computers. Instead, we do anticipate the hybrid tensor network would find its application in specific problems with certain properties whose accurate solutions are hard with classical tensor network theory and resource-demanding with conventional quantum simulation algorithms. We discuss potential applications of hybrid TTN in the next section.

V. APPLICATIONS

Hybrid tensor networks may have wide applications in quantum computing and quantum simulation for solving different physics problems. The key benefit of a hybrid tensor network is to more efficiently represent a multipartite quantum state so that the required quantum resource is significantly reduced with the help of classical computers. The hybrid tensor network would bolster up the power of near-term quantum computers so that the limitation on the number of controllable qubits of NISQ devices could be greatly alleviated. Meanwhile, hybrid tensor networks may find their applications in fault-tolerant quantum computing as well, where the number of logical qubits could also be limited owing to the huge overhead for error correction. In this section, we discuss potential applications of hybrid tensor networks in different physics problems, ranging from chemistry, many-body physics, quantum field theory, to quantum gravity. We only summarize the ideas here and refer to the Appendix for details.

- *Quantum chemistry.* As we have discussed in

Sec. III, ideas corresponding to simple hybrid tree tensor networks of Fig. 3(b,c) have been studied for representing excited energy eigenstates [20] and active + virtual orbitals [9] in electronic structure calculation. While the scheme in Ref. [9] assumed the configuration interaction ansatz for the virtual orbitals, a general classical tensor network may be used instead to improve the approximation. We refer to Ref. [29] to recent studies of TN approaches to quantum chemistry. Another potential application of the hybrid tensor network is to go beyond the BornOppenheimer (BO) approximation, which may have applications in understanding radiationless decay between electronic states [30], relativistic effects [31], or conical intersections [32–34]. By separately storing the electrons and nuclei with quantum processors and their correlations with a classical (quantum) tensor, we can probe effects beyond the BO approximation by manipulating quantum states only of the electrons or the nuclei.

- *Quantum many-body physics.* Many interesting quantum phenomena could be captured by the model of weakly or moderately coupled subsystems. When each subsystem has strong interactions, such as electrons with multiple degrees of freedom in strongly correlated materials, classical algorithms might fail to work, and quantum simulation with hybrid tensor networks could be used instead for exploring emergent quantum phenomena [35–38]. For example, our method can be applied for searching Majorana zero-modes and topological phase transitions [39–43, 60]. Considering a bulk model Hamiltonian with boundary conditions between superconductors and topological insulators, we are able to drive the superconductor heterostructures into topologically non-trivial phases by tuning the coupling and bulk properties. Successful simulation of such systems might provide an avenue of systematic searches for topological superconductivity from potential candidates.
- *Quantum field theories.* Quantum simulation has been applied to study the scattering problem in quantum field theory with the Jordan-Lee-Preskill algorithm [44, 45]. Directly implementing this algorithm may require too many qubits that are beyond the capability of current and near-future quantum computers. This is especially important when we wish to study scattering processes with sufficiently high initial energy, which should be, in principle, highly quantum processes with significant particle productions. Quantum simulation with hybrid tensor networks might be useful, for instance, in the regime where the coupling is moderate so that we could split the whole system into smaller subsystems and only use a quantum processor to represent the subsystems.
- *Quantum gravity.* Conceptual connections have

been recently revealed between quantum gravity thought experiments and quantum information science, including ones between quantum chaos and quantum black holes [46], quantum error correction and holography [47], quantum complexity and gravitational action [48], quantum Church-Turing Thesis and black hole firewalls [49], etc. Although these works might unravel fundamental puzzles about black hole information, they require crucial demands on the power of quantum computers. Quantum algorithms with hybrid tensor networks might resolve this problem for near-term quantum computing. We consider the example of the traversable wormhole [50, 51], which in the quantum information language, could be interpreted as a novel teleportation scheme transforming quantum information from one side of thermofield double to the other side, dual to a traversable wormhole gravitational system in the holographic description. In the regime with relatively low temperature (for instance, where the black hole is near extremal), one could consider using hybrid tensor networks to perform the simulation with only one side of the thermofield double stored with a quantum computer.

VI. SUMMARY

In this work, we propose a framework of the hybrid tensor network and studied its application in variational quantum simulation. Targeting at practical problems that have both classical and genuine quantum effects, hybrid tensor networks integrate the power of classical tensor network theories and quantum computing, and hence enable quantum simulation of large-scale problems with small quantum processors. While this work numerically verifies variational quantum simulation with hybrid tree tensor networks in finding the ground state energy of 1D and 2D spin systems, the theory applies to general scenarios, such as real-time dynamics and general physics systems. In particular, practical investigations

of our method in quantum chemistry, quantum many-body physics, quantum field theory, and quantum gravity thought experiments would be interesting future works. There also exist other powerful classical methods, such as quantum Monte Carlo methods [52, 53] and machine learning with neural networks [54, 55], and an interesting future direction is to investigate the combination of these methods with quantum computing. Another independent approach of simulating large quantum systems with small quantum computers is to decompose multi-qubit gates into a mixture of single-qubit gates so that the circuit becomes a mixture of circuits with gates only locally applied to subsets of qubits [56–58]. The combination of these methods and ours may lead to further advantages. Demonstrating quantum advantage over supercomputers in certain tasks — quantum supremacy — has been experimentally realized [59]. The next milestone is to demonstrate the quantum advantage in solving practically meaningful and classically intractable tasks. While current quantum devices are still insufficient, our work may shed light on the avenue for achieving this goal with near-term noisy intermediate-scale quantum hardware.

ACKNOWLEDGEMENT

We thank Suguru Endo, Patrick Hayden, Arthur Jaffe, Sam McArdle, John Preskill, Vlatko Vedral for insightful, related discussions and comments. J.S. acknowledges support from the China Scholarship Council (CSC). J.L. is supported in part by the Institute for Quantum Information and Matter (IQIM), an NSF Physics Frontiers Center (NSF Grant PHY-1125565) with support from the Gordon and Betty Moore Foundation (GBMF-2644), and by the Walter Burke Institute for Theoretical Physics. Q.Z. acknowledges the support by the Department of Defense through the Hartree Postdoctoral Fellowship at QuICS. Y.Z. was supported in part by the Templeton Religion Trust under grant TRT 0159 and by the ARO under contract W911NF1910302.

-
- [1] S. R. White, *Phys. Rev. Lett.* **69**, 2863 (1992).
 - [2] S. Rommer and S. Östlund, *Phys. Rev. B* **55**, 2164 (1997).
 - [3] R. Orús, *Nature Reviews Physics* **1**, 538 (2019).
 - [4] R. P. Feynman, *International Journal of Theoretical Physics* **21**, 467 (1982).
 - [5] S. McArdle, S. Endo, A. Aspuru-Guzik, S. C. Benjamin, and X. Yuan, *Rev. Mod. Phys.* **92**, 015003 (2020).
 - [6] Y. Cao, J. Romero, J. P. Olson, M. Degroote, P. D. Johnson, M. Kieferová, I. D. Kivlichan, T. Menke, B. Peropadre, N. P. Sawaya, *et al.*, *Chemical reviews* **119**, 10856 (2019).
 - [7] J. O’Gorman and E. T. Campbell, *Phys. Rev. A* **95**, 032338 (2017).
 - [8] J. Preskill, *Quantum* **2**, 79 (2018).
 - [9] T. Takeshita, N. C. Rubin, Z. Jiang, E. Lee, R. Babbush, and J. R. McClean, *Phys. Rev. X* **10**, 011004 (2020).
 - [10] F. Barratt, J. Dborin, M. Bal, V. Stojevic, F. Pollmann, and A. G. Green, arXiv preprint arXiv:2003.12087 (2020).
 - [11] X. Yuan, S. Endo, Q. Zhao, Y. Li, and S. C. Benjamin, *Quantum* **3**, 191 (2019).
 - [12] L. Hackl, T. Guaita, T. Shi, J. Haegeman, E. Demler, and I. Cirac, arXiv preprint arXiv:2004.01015 (2020).
 - [13] U. Schollwöck, *Annals of Physics* **326**, 96 (2011).
 - [14] M. Fannes, B. Nachtergaele, and R. F. Werner, *Communications in mathematical physics* **144**, 443 (1992).

- [15] A. Klumper, A. Schadschneider, and J. Zittartz, *Journal of Physics A: Mathematical and General* **24**, L955 (1991).
- [16] A. Klümper, A. Schadschneider, and J. Zittartz, *EPL (Europhysics Letters)* **24**, 293 (1993).
- [17] F. Verstraete and J. I. Cirac, arXiv preprint cond-mat/0407066 (2004).
- [18] Y.-Y. Shi, L.-M. Duan, and G. Vidal, *Phys. Rev. A* **74**, 022320 (2006).
- [19] G. Vidal, *Phys. Rev. Lett.* **99**, 220405 (2007).
- [20] J. R. McClean, M. E. Kimchi-Schwartz, J. Carter, and W. A. de Jong, *Phys. Rev. A* **95**, 042308 (2017).
- [21] J. I. Colless, V. V. Ramasesh, D. Dahlen, M. S. Blok, M. E. Kimchi-Schwartz, J. R. McClean, J. Carter, W. A. de Jong, and I. Siddiqi, *Phys. Rev. X* **8**, 011021 (2018).
- [22] J. R. McClean, Z. Jiang, N. C. Rubin, R. Babbush, and H. Neven, *Nature Communications* **11**, 1 (2020).
- [23] J. M. Bowman, *Science* **319**, 40 (2008).
- [24] X. Chen, Z.-C. Gu, and X.-G. Wen, *Phys. Rev. B* **82**, 155138 (2010).
- [25] X. Chen, Z.-C. Gu, and X.-G. Wen, *Phys. Rev. B* **83**, 035107 (2011).
- [26] Y. Gu, X.-L. Qi, and D. Stanford, *JHEP* **05**, 125 (2017), arXiv:1609.07832 [hep-th].
- [27] S. Chandrasekhar, *The mathematical theory of black holes*, Vol. 69 (Oxford University Press, 1998).
- [28] S. McArdle, T. Jones, S. Endo, Y. Li, S. C. Benjamin, and X. Yuan, *npj Quantum Information* **5**, 1 (2019).
- [29] S. Szalay, M. Pfeffer, V. Murg, G. Barcza, F. Verstraete, R. Schneider, and Ö. Legeza, *International Journal of Quantum Chemistry* **115**, 1342 (2015).
- [30] G. A. Worth and L. S. Cederbaum, *Annu. Rev. Phys. Chem.* **55**, 127 (2004).
- [31] M. Reiher and A. Wolf, *Relativistic quantum chemistry: the fundamental theory of molecular science* (John Wiley & Sons, 2014).
- [32] W. Domcke, D. R. Yarkony, and H. Köppel, *Conical Intersections* (WORLD SCIENTIFIC, 2004) <https://www.worldscientific.com/doi/pdf/10.1142/5406>.
- [33] W. Domcke and D. R. Yarkony, *Annu. Rev. Phys. Chem.* **63**, 325 (2012), pMID: 22475338, <https://doi.org/10.1146/annurev-physchem-032210-103522>.
- [34] I. G. Ryabinkin, L. Joubert-Doriol, and A. F. Izmaylov, *Acc. Chem. Res.* **50**, 1785 (2017), pMID: 28665584, <https://doi.org/10.1021/acs.accounts.7b00220>.
- [35] M. Sato and Y. Ando, *Reports on Progress in Physics* **80**, 076501 (2017).
- [36] A. V. Chubukov, D. Efremov, and I. Eremin, *Physical Review B* **78**, 134512 (2008).
- [37] R. Fernandes, A. Chubukov, and J. Schmalian, *Nature physics* **10**, 97 (2014).
- [38] P. Dai, *Reviews of Modern Physics* **87**, 855 (2015).
- [39] R. M. Lutchyn, J. D. Sau, and S. D. Sarma, *Physical review letters* **105**, 077001 (2010).
- [40] R. t. Lutchyn, E. Bakkers, L. P. Kouwenhoven, P. Krogstrup, C. Marcus, and Y. Oreg, *Nature Reviews Materials* **3**, 52 (2018).
- [41] A. Y. Kitaev, *Physics-Uspexhi* **44**, 131 (2001).
- [42] J. Alicea, *Reports on progress in physics* **75**, 076501 (2012).
- [43] C. Beenakker, *Annu. Rev. Condens. Matter Phys.* **4**, 113 (2013).
- [44] S. P. Jordan, K. S. Lee, and J. Preskill, *Science* **336**, 1130 (2012), arXiv:1111.3633 [quant-ph].
- [45] S. P. Jordan, K. S. Lee, and J. Preskill, *Quant. Inf. Comput.* **14**, 1014 (2014), arXiv:1112.4833 [hep-th].
- [46] P. Hayden and J. Preskill, *JHEP* **09**, 120 (2007), arXiv:0708.4025 [hep-th].
- [47] X. Dong, D. Harlow, and A. C. Wall, *Phys. Rev. Lett.* **117**, 021601 (2016), arXiv:1601.05416 [hep-th].
- [48] A. R. Brown, D. A. Roberts, L. Susskind, B. Swingle, and Y. Zhao, *Phys. Rev. Lett.* **116**, 191301 (2016), arXiv:1509.07876 [hep-th].
- [49] I. Kim, E. Tang, and J. Preskill, (2020), arXiv:2003.05451 [hep-th].
- [50] P. Gao, D. L. Jafferis, and A. C. Wall, *JHEP* **12**, 151 (2017), arXiv:1608.05687 [hep-th].
- [51] J. Maldacena, D. Stanford, and Z. Yang, *Fortsch. Phys.* **65**, 1700034 (2017), arXiv:1704.05333 [hep-th].
- [52] W. M. C. Foulkes, L. Mitas, R. J. Needs, and G. Rajagopal, *Rev. Mod. Phys.* **73**, 33 (2001).
- [53] J. Carlson, S. Gandolfi, F. Pederiva, S. C. Pieper, R. Schiavilla, K. E. Schmidt, and R. B. Wiringa, *Rev. Mod. Phys.* **87**, 1067 (2015).
- [54] G. Carleo and M. Troyer, *Science* **355**, 602 (2017).
- [55] Y. Li, arXiv preprint arXiv:1701.07274 (2017).
- [56] T. Peng, A. Harrow, M. Ozols, and X. Wu, arXiv preprint arXiv:1904.00102 (2019).
- [57] K. Mitarai and K. Fujii, arXiv preprint arXiv:1909.07534 (2019).
- [58] K. Mitarai and K. Fujii, arXiv e-prints, arXiv:2006.11174 (2020).
- [59] F. Arute, K. Arya, R. Babbush, D. Bacon, J. C. Bardin, R.arends, R. Biswas, S. Boixo, F. G. Brandao, D. A. Buell, et al., *Nature* **574**, 505 (2019).
- [60] J. D. Sau, S. Tewari, R. M. Lutchyn, T. D. Stanescu, and S. D. Sarma, *Physical Review B* **82**, 214509 (2010).
- [61] J. Maldacena and X.-L. Qi, (2018), arXiv:1804.00491 [hep-th].
- [62] B. Yoshida and A. Kitaev, (2017), arXiv:1710.03363 [hep-th].
- [63] J. Maldacena and L. Susskind, *Fortsch. Phys.* **61**, 781 (2013), arXiv:1306.0533 [hep-th].
- [64] S. H. Shenker and D. Stanford, *JHEP* **03**, 067 (2014), arXiv:1306.0622 [hep-th].
- [65] J. Maldacena and D. Stanford, *Phys. Rev. D* **94**, 106002 (2016), arXiv:1604.07818 [hep-th].
- [66] J. M. Maldacena, *Int. J. Theor. Phys.* **38**, 1113 (1999), arXiv:hep-th/9711200.
- [67] B. Yoshida and N. Y. Yao, *Phys. Rev. X* **9**, 011006 (2019), arXiv:1803.10772 [quant-ph].
- [68] A. R. Brown, H. Gharibyan, S. Leichenauer, H. W. Lin, S. Nezami, G. Salton, L. Susskind, B. Swingle, and M. Walter, (2019), arXiv:1911.06314 [quant-ph].

Appendix A: Hybrid tensor network

As shown in the main text, the hybrid tensor network consists of classical and quantum tensors, whose mathematical definition is consistent with that of the conventional tensor network. That is, tensor contractions are mathematically defined the same for classical and quantum tensors. Nevertheless, we distinguish them because operationally, classical tensors are contracted classically via tensor multiplication, while quantum tensors are contracted via measuring a quantum state on a quantum computer. In the following, we elaborate on the detailed definition of classical and quantum tensors, the definition of tensor contraction and its meaning, the way to measure local observables, and the application in quantum simulation.

1. Classical and quantum tensors

A general rank- n tensor is a multi-dimensional array with n indices denoted as T_{i_1, i_2, \dots, i_n} . In quantum mechanics, it represents the wave function of an n -partite quantum state in the computational basis,

$$|\psi\rangle = \sum_{j_1, j_2, \dots, j_n} \psi_{j_1, j_2, \dots, j_n} |j_1\rangle |j_2\rangle \dots |j_n\rangle. \quad (\text{A1})$$

We can see that directly storing a general quantum state in a classical memory is highly inefficient, which in general costs exponential space resources with respect to the number of parties. This thus motivates us to find more efficient ways to represent quantum states.

The deep observation of physicists is that quantum states in nature may only lie in a small subset of the whole Hilbert space, where the area law scaling may exist, for example, with the ground state of certain gaped local Hamiltonians. It thus enables the possibility of efficient classical representation of these quantum states. The overall idea is to decompose the rank- n tensor into a network of low-rank tensors. Take the matrix product state (MPS) ansatz as an example, as shown in Fig. 6(a), the rank- n tensor is now decomposed into n low-rank tensors as

$$|\psi\rangle = \sum_{j_1, j_2, \dots, j_n} \text{Tr}[\alpha_1^{j_1} \dots \alpha_n^{j_n}] |j_1\rangle |j_2\rangle \dots |j_n\rangle. \quad (\text{A2})$$

Here each α_k is a rank-3 tensor (except for α_1 and α_n whose rank is 2), and the index j_k is the physical index, with dimension 2 for the qubit case. The other two indices (or one index for α_1, α_n) are called the bond indices with dimension χ , normally being a constant number. Here the trace operation in Eq. (A2) is for the bond indices.

It is clear that the entanglement of any local subsystem is upper bounded by 2χ , where 2 accounts for the two boundaries and χ for the contribution from each boundary, as shown in Fig. 6(b). Note that the MPS representation thus compresses the space of the n -partite state from $O(2^n)$ to $O(n\chi^2)$, which is from exponential to linear with the particle number n . This tremendous reduction is based on the pre-knowledge of the weakly entangled state under the geometrically local interactions. However, typically the quantum state in the large Hilbert space could be highly entangled, such as excited eigenstates and states after quenched dynamics of the chaotic Hamiltonian. Many different classical tensor networks have been proposed for different problems. Nevertheless, it would be likely that

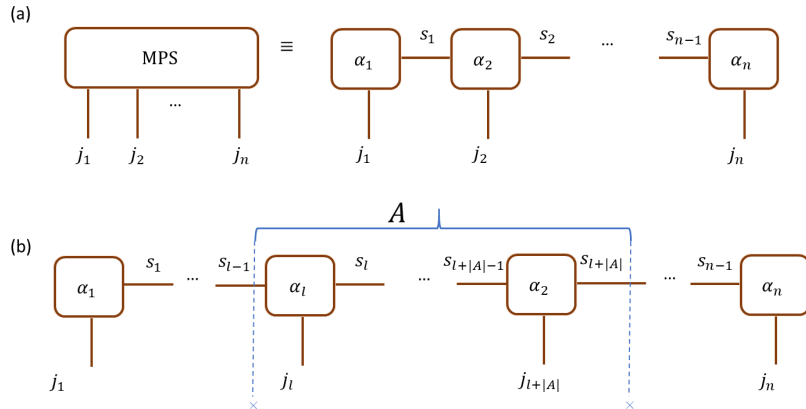


FIG. 6. Illustration of a typical classical tensor network — the matrix product state.

certain quantum systems, such as the electronic structure in chemistry and the Hubbard model, may not be efficiently described via any classical method.

It thus motivates the idea of quantum simulation, i.e., using a controllable quantum system to simulate a target quantum problem. A quantum state generated from applying a unitary circuit to a certain initial state forms an intrinsic large-rank quantum tensor and can be naturally stored and manipulated with a quantum computer. As an alternative approach, several quantum algorithms have been proposed to solve either static or dynamic problems of a general many-body problem. In literature, classical tensor network theory and quantum simulation are generally used as separate techniques in classical and quantum computing. Here, we introduce quantum tensors to be general n -partite quantum states prepared by a quantum computer and classical tensors to low-rank tensors stored in a classical computer and show the combination of quantum and classical tensors as a hybrid tensor network.

Suppose we generate an n -partite quantum state by applying a unitary U_ψ to an initial state $|\bar{0}\rangle$ as $|\psi\rangle = U_\psi |\bar{0}\rangle$. As shown in Eq. (A1), the quantum state can be regarded as a rank- n tensor in the computational basis. We can also introduce classical index to the quantum state by applying different unitary gates as

$$|\psi^i\rangle = U_{\psi^i} |\bar{0}\rangle = \sum_{j_1, j_2, \dots, j_n} \psi_{j_1, j_2, \dots, j_n}^i |j_1\rangle |j_2\rangle \dots |j_n\rangle. \quad (\text{A3})$$

Alternatively, we can also apply the same unitary but to different initial states as

$$|\psi^i\rangle = U |\bar{0}^i\rangle = \sum_{j_1, j_2, \dots, j_n} \psi_{j_1, j_2, \dots, j_n}^i |j_1\rangle |j_2\rangle \dots |j_n\rangle, \quad (\text{A4})$$

where the classical index i indicates the different unitaries or different initial states. As a result, it as a whole forms a rank- $(n+1)$ tensor $\Psi_{j_1, j_2, \dots, j_n}^i$. For simplicity, we only introduce one classical index here, and it is clear that there is no restriction to introduce more classical indices. We regard all these cases as quantum tensors, and the network connected with quantum tensors and classical tensors as a hybrid tensor network. Hereafter, we put indices corresponding to classical labels and quantum basis to the superscript and subscript of the tensor, respectively.

2. Hybrid tensor network

Here we show how to connect quantum and classical tensors to form a hybrid tensor. When connecting two tensors, being either classical or quantum, we follow the conventional rule for tensor contraction. While the mathematical definition of tensor contraction of a hybrid tensor network is consistent with the conventional definition, its practical meaning can be different. Depending on whether the tensor and the index are quantum or classical, there are five different cases under contraction. To ease the explanation, w.o.l.g., we consider contraction of rank-2 classical tensors and rank- $(n+1)$ quantum tensors. We also use \dots to abbreviate the quantum indices when they are not contracted.

- Case 1: quantum tensor (contracted index: classical) & classical tensor (contracted index: classical).

First, we combine a quantum tensor $\psi_{\dots}^{i_1}$ with a classical tensor α^{i_1, i_2} to form a new rank- $(n+1)$ tensor,

$$\tilde{\psi}_{\dots}^{i_2} = \sum_{i_1} \psi_{\dots}^{i_1} \cdot \alpha^{i_1, i_2}, \quad (\text{A5})$$

where the contracted index from the quantum and classical tensors is a classical label. To understand the meaning of Eq. (A5), we regard the quantum tensor $\psi_{\dots}^{i_1}$ as a set of independent quantum states $\{|\psi^{i_1}\rangle\}$ and the tensor $\tilde{\psi}_{\dots}^{i_2}$ represents a new set of states

$$|\tilde{\psi}^{i_2}\rangle = \sum_{i_1} \alpha^{i_1, i_2} |\psi^{i_1}\rangle, \quad (\text{A6})$$

where each one is now a superposition of the original states $\{|\psi^{i_1}\rangle\}$. As a special case, when the classical tensor is rank-1, α^{i_1} , the output tensor is

$$|\tilde{\psi}\rangle = \sum_{i_1} \alpha^{i_1} |\psi^{i_1}\rangle. \quad (\text{A7})$$

Therefore, we can connect a classical tensor to the classical index of a quantum tensor to effectively represent a superposition of quantum states.

- Case 2: quantum tensor (contracted index: quantum) & classical tensor (contracted index: classical).

When the contracted index i_1 of the quantum tensor $\psi_{i_1, \dots}$ corresponds to a quantum system, the tensor contraction is similarly defined as

$$\tilde{\psi}^{i_2} = \sum_{i_1} \psi_{i_1, \dots} \cdot \alpha^{i_1, i_2}. \quad (\text{A8})$$

When considering quantum states, the contraction transforms an input state $|\psi\rangle$ to a set of output states $\{|\tilde{\psi}^{i_2}\rangle\}$ as

$$|\tilde{\psi}^{i_2}\rangle = \sum_{i_1} \alpha^{i_1, i_2} \langle i_1 | \psi \rangle, \quad (\text{A9})$$

which is equivalent to projecting the contracted system onto $|i_1\rangle$ to form a set of un-normalized states $|\psi^{i_1}\rangle = \langle i_1 | \psi \rangle$ and re-combining them with coefficients α^{i_1, i_2} . Actually, if we regard α as a unitary gate with i_2 representing a quantum system, it corresponds to a local unitary transformation of the state.

- Case 3: quantum tensor (contracted index: classical) & quantum tensor (contracted index: classical).

Next, we consider the contraction of two quantum tensors with the contracted index being classical for both tensors. Suppose the two quantum tensors are ψ_{\dots}^i and ϕ_{\dots}^i , the contraction of index i gives

$$\tilde{\psi}_{\dots} = \sum_i \psi_{\dots}^i \cdot \phi_{\dots}^i. \quad (\text{A10})$$

Considering quantum states, the contraction transforms two sets of states $\{|\psi^i\rangle\}$ and $\{|\phi^i\rangle\}$ to an un-normalized state

$$|\tilde{\psi}\rangle = \sum_i |\psi^i\rangle \otimes |\phi^i\rangle. \quad (\text{A11})$$

By contracting two quantum tensors, we can thus effectively entangle two quantum systems. We can also add a classical tensor in between so that the amplitude for each $|\psi^i\rangle \otimes |\phi^i\rangle$ is different.

- Case 4: quantum tensor (contracted index: quantum) & quantum tensor (contracted index: classical).

When one of the contracted indices corresponds to a quantum system, the contraction is similarly defined as

$$\tilde{\psi}_{\dots} = \sum_i \psi_{i, \dots} \cdot \phi_{\dots}^i. \quad (\text{A12})$$

Considering quantum states, the contraction converts $|\psi\rangle$ and $\{|\phi^i\rangle\}$ to

$$|\tilde{\psi}\rangle = \sum_i \langle i | \psi \rangle \otimes |\phi^i\rangle. \quad (\text{A13})$$

Again, this is equivalent to applying a projection to $|\psi\rangle$ to get a set of states $\{|\psi^i\rangle = \langle i | \psi \rangle\}$ and then connecting the classical indices of the two quantum tensors.

- Case 5: quantum tensor (contracted index: quantum) & quantum tensor (contracted index: quantum).

When both contracted indices represent for quantum systems, we contract two quantum tensors $\psi_{i, \dots}$ and $\phi_{i, \dots}$ as

$$\tilde{\psi}_{\dots} = \sum_i \psi_{i, \dots} \cdot \phi_{i, \dots}. \quad (\text{A14})$$

In the quantum state language, it is equivalent to

$$|\tilde{\phi}\rangle = \sum_i \langle i | \psi \rangle \otimes \langle i | \phi \rangle = \sum_i \langle i, i | \psi \rangle \otimes |\phi\rangle. \quad (\text{A15})$$

which accounts for a Bell state projection on the contracted systems. Note that since it is a measurement on both states, the success probability could be less than 1. Then if there are multiple contractions of quantum indices, the overall probability will be exponentially small. Therefore, we only allow a constant number of contractions of two quantum indices in the hybrid tensor network.

For a general hybrid tensor network consisting of classical and quantum tensors, the tensor contraction rule and its meaning with respect to the quantum state follow similarly by sequentially applying the above cases.

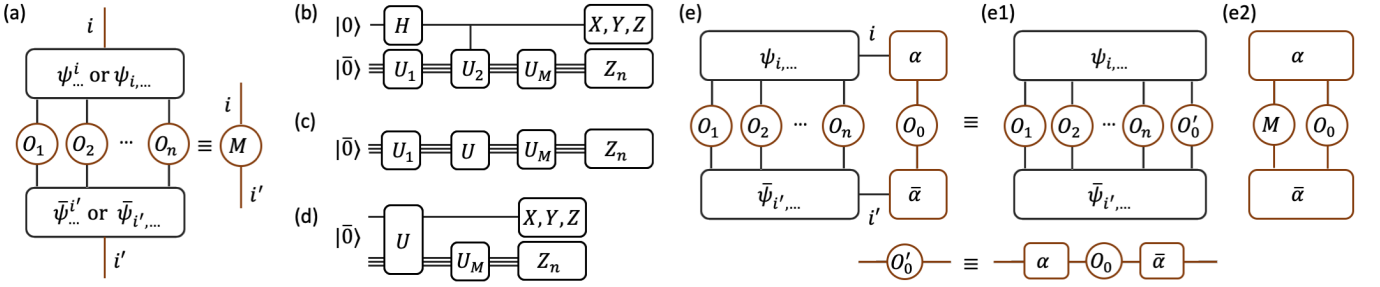


FIG. 7. Measuring expectation values of a quantum tensor. Same as Fig. 2 in the main text.

3. Calculation of expectation values of local observables

Given a hybrid tensor network representation of a quantum state, we now show how to measure the expectation values of tensor products of local observables. Here we only show the basic rules and whether the calculation is efficient highly depends on the structure of the hybrid tensor network, the same as the scenario of the conventional tensor network. The basic rule follows the same mathematics of tensor contraction. Therefore, for classical tensors, the expectation value is calculated in the same way as conventional tensor networks. While for quantum tensors, we can no longer calculate the expectation value via tensor contraction since it involves matrix multiplication of a rank- n tensor. Instead, we calculate the expectation value with a quantum computer by preparing the state and measuring it.

As shown in Fig. 7(a), we consider the expectation value on the n quantum systems of a rank- $(n+1)$ quantum tensor. This tensor can be either an n -partite quantum state with a classical index i or an $(n+1)$ -partite quantum state with a quantum basis index i . By measuring the n systems, it gives a new rank 2 tensor $M^{i',i}$ with two open indices i and i' ,

$$M^{i',i} = \langle \psi^{i'} | O_1 \otimes O_2 \otimes \cdots \otimes O_n | \psi^i \rangle. \quad (\text{A16})$$

Here the definition is the same if we measure an $(n+1)$ -partite quantum state. We always put the indices of $M^{i',i}$ to the superscript, because the measurement observable is always a classical low-rank tensor. Note that the matrix $M^{i',i}$ is always hermitian so that it can be measured when the indices i and i' are contracted to another quantum tensor. Now we show how to get $M^{i',i}$ for different cases.

- The rank- $(n+1)$ quantum tensor is an n -partite quantum state with a classical index i .
 - Suppose $|\psi^i\rangle = U^i |\bar{0}\rangle$, $U_1 = U^i$. We measure $M^{i',i}$ with the quantum circuit in Fig. 7(b). Consider $U_2 = U^{i'} (U^i)^\dagger$ and U_M to be the unitary that rotates the eigenstates of the observable to the computational basis. The output state before the U_M gate is

$$|\tilde{\psi}\rangle = \frac{1}{\sqrt{2}} (|0\rangle |\psi^i\rangle + |1\rangle |\psi^{i'}\rangle). \quad (\text{A17})$$

When the ancillary qubit measures the Pauli X , Y , Z operators, and the n -partite system measures $M = O_1 \otimes O_2 \otimes \cdots \otimes O_n$, the expectation values are

$$\begin{aligned} \langle \tilde{\psi} | X \otimes M | \tilde{\psi} \rangle &= \frac{1}{2} (M^{2,1} + M^{1,2}), \\ \langle \tilde{\psi} | Y \otimes M | \tilde{\psi} \rangle &= \frac{1}{2} (iM^{2,1} - iM^{1,2}), \\ \langle \tilde{\psi} | Z \otimes M | \tilde{\psi} \rangle &= \frac{1}{2} (M^{1,1} - M^{2,2}). \end{aligned} \quad (\text{A18})$$

Note that $M^{1,2}$ is the complex conjugate of $M^{2,1}$, and we have

$$\langle \tilde{\psi} | I \otimes M | \tilde{\psi} \rangle = \frac{1}{2} (M^{1,1} + M^{2,2}), \quad (\text{A19})$$

which can be obtained from the measurement of any Pauli basis. Therefore we can exactly solve each term $M^{i,j}$ ($i, j = 1, 2$) and construct the measurement

$$\tilde{M} = \begin{Bmatrix} M^{1,1} & M^{1,2} \\ M^{2,1} & M^{2,2} \end{Bmatrix}$$

– Suppose $|\psi^i\rangle = U|\bar{0}^i\rangle$. We measure $M^{i',i}$ with the quantum circuit in Fig. 7(c). Now we need to input $(|\bar{0}^i\rangle \pm |\bar{0}^{i'}\rangle)/\sqrt{2}$ and $(|i\rangle \pm i|i'\rangle)/\sqrt{2}$ and the matrix elements can be similarly obtained.

- The rank- $(n+1)$ quantum tensor is an $n+1$ -partite quantum state.

We need to measure

$$M^{i',i} = \langle \psi | |i'\rangle \langle i| \otimes O_1 \otimes O_2 \otimes \cdots \otimes O_n \otimes |\psi\rangle = \langle \psi | (|i'\rangle \langle i|) \otimes O_1 \otimes O_2 \otimes \cdots \otimes O_n | \psi \rangle. \quad (\text{A20})$$

Note that the matrix $|i'\rangle \langle i|$ can always be represented as a linear combination of the Pauli operators, we can thus instead measure the uncontracted qubit in the three X, Y, Z Pauli bases to equivalently get any $M^{i',i}$ as shown in Fig. 7(d). Suppose $|\psi\rangle = U|\bar{0}\rangle$, we denote

$$E(\sigma) = \langle \psi | \sigma \otimes O_1 \otimes O_2 \otimes \cdots \otimes O_n | \psi \rangle, \quad (\text{A21})$$

and we can reconstruct the measurement \tilde{M} as

$$\tilde{M} = \frac{1}{2}(E(I)I + E(X)X - E(Y)Y + E(Z)Z), \quad (\text{A22})$$

where $E(X), E(I), E(Y), E(Z)$ are the obtained expectation values with Pauli measurements I, X, Y, Z .

Calculating the expectation value of a general hybrid tensor network follows the above basic rules for classical and quantum tensors. Nevertheless, similar to the conventional tensor network, different orders of tensor contraction could have different procedures and complexities. For example, say that we are considering the hybrid tensor shown in Fig. 7(e), which consists of a rank- $(n+1)$ quantum tensor and a classical tensor. We could first contract the right classical observable O_0 with classical tensor α , and obtain a new observable O'_0 . Then we measure the $n+1$ -partite quantum state to get the final expectation value. Here we need classical contraction and a single local measurement with repetition samples \mathcal{M} . This procedure is shown in Fig. 7(e1). Alternatively, we can also use the circuit in Fig. 7(d) to reconstruct observable M by measuring the $n+1$ -partite quantum state and then contract the classical tensors. This procedure requires three local measurement settings (X, Y , and Z on the first qubit) with total repetition samples of $3\mathcal{M}$.

4. Application in variational quantum simulation

The hybrid tensor network provides a way to more efficiently represent quantum states with fewer quantum resources. When using the hybrid tensor network, it can be applied in variational quantum simulation for solving static energy spectra and simulating the dynamic time evolution of a quantum system.

We consider a many-body Hamiltonian

$$H = \sum_i \lambda_i h_i \quad (\text{A23})$$

with coefficients λ_i and tensor products of Pauli matrices h_i . To find the ground state of the Hamiltonian, we consider a parameterized hybrid quantum tensor network, which corresponds to a possibly un-normalized state $|\psi(\vec{x})\rangle$. Here \vec{x} denotes the parameters that can be changed in the hybrid tensor network, which includes the parameterized angles in the quantum circuit and parameters in the classical tensors. Then we can measure the average energy as

$$E(\vec{x}) = \frac{\langle \psi(\vec{x}) | H | \psi(\vec{x}) \rangle}{\langle \psi(\vec{x}) | \psi(\vec{x}) \rangle} = \frac{\sum_i \lambda_i \langle \psi(\vec{x}) | h_i | \psi(\vec{x}) \rangle}{\langle \psi(\vec{x}) | \psi(\vec{x}) \rangle}, \quad (\text{A24})$$

where each $\langle \psi(\vec{x}) | h_i | \psi(\vec{x}) \rangle$ or the normalization $\langle \psi(\vec{x}) | \psi(\vec{x}) \rangle$ can be obtained by calculating the expectation value of the hybrid tensor network with the method we discussed in the previous section. Having measured $E(\vec{x})$ for any \vec{x} , we can then optimize the parameter space via the classical algorithm to minimize $E(\vec{x})$ to search for the ground state.

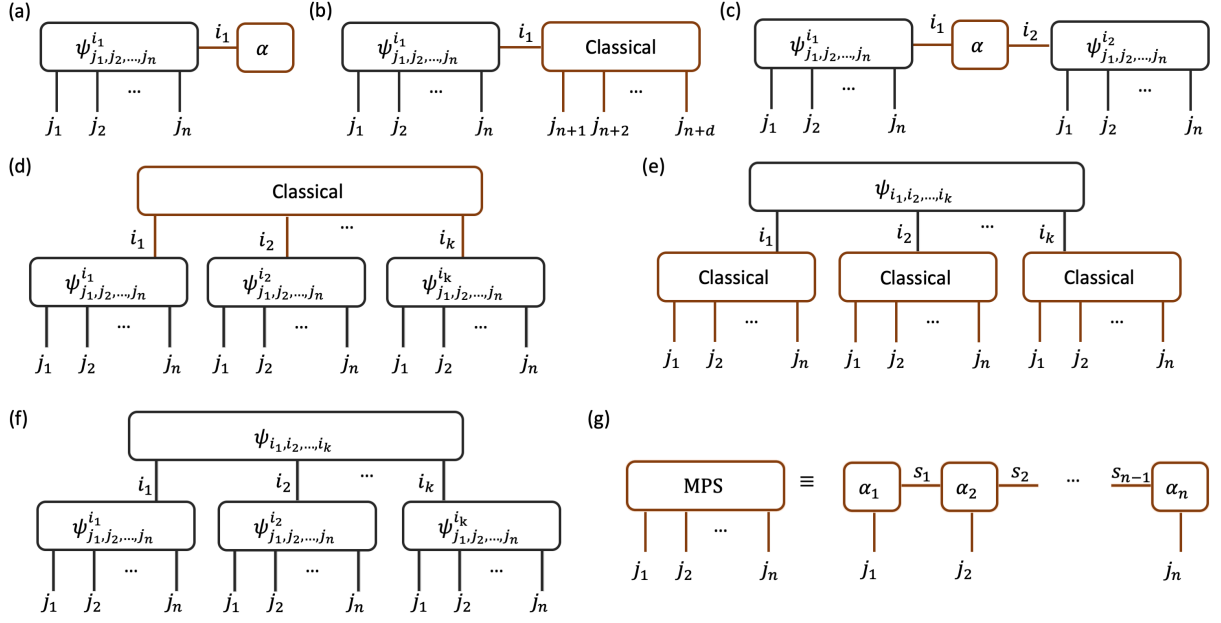


FIG. 8. Hybrid quantum-classical tensor network. (a) We can extend the power of a quantum state by adding a classical tensor as in Eq. (B1). (b) We can combine a quantum state and a classical tensor to represent a state in a larger Hilbert space as in Eq. (B7). (c) We can use a classical tensor to connect two quantum states as in Eq. (B10). (d) A quantum-classical hybrid tensor as in Eq. (B12). (e) A classical-quantum hybrid tensor as in Eq. (B15). (f) A quantum-quantum hybrid tensor as in Eq. (B18). (g) A commonly-used classical tensor network MPS.

We note that the whole optimization procedure is identical to the conventional approach called variational quantum eigensolver. The difference lies in the usage of the hybrid tensor network, which may enable quantum simulation of large systems with small quantum processors. We can also use the hybrid tensor network for simulating Hamiltonian dynamics. The circuit for the implementation of variational Hamiltonian simulation with hybrid tensor networks is slightly more complicated, and we leave the discussion to follow-up works. In the following, we mainly focus on using the hybrid tensor network for finding the ground state of Hamiltonians.

Appendix B: Hybrid tree tensor network

Calculating a general hybrid tensor network can be costly. Here we expand the discussion of the main text and focus on hybrid tensor networks with a tree structure. We first consider examples of hybrid tree tensor networks (TNN) and discuss its application in representing correlations of the multipartite quantum state. We then study the cost of calculating the expectation values of a general hybrid TNN. We also study the entanglement property and correlation of the quantum state represented by the hybrid TNN.

1. Example of hybrid tree tensor networks

We show several examples of hybrid tree tensor networks in Fig. 8. In the following, we discuss the application of each tensor network and its connection with existing results. For each n -partite state, we assume it is an n -qubit parameterized state $|\psi(\vec{\theta})\rangle$, obtained by applying a sequence of local gates as $|\psi(\vec{\theta})\rangle = \prod_j U_j(\theta_j) |\bar{0}\rangle$ with an initial state $|\bar{0}\rangle$ and parameters $\vec{\theta} = \{\theta_j\}$.

a. Extending the power of the quantum state

Suppose we use the quantum state $|\psi(\vec{\theta})\rangle$ as a potential solution to the n -qubit problem. We can regard the quantum state as a pure rank- n quantum tensor. A simple way to extend the capability of the rank- n quantum tensor

is to concatenate a classical tensor α^i to it as

$$|\psi(\vec{x})\rangle = \sum_i \alpha^i |\psi^i(\vec{\theta}_i)\rangle, \quad (\text{B1})$$

where each $|\psi^i(\vec{\theta}_i)\rangle$ can be regarded as different rank- n quantum tensors and $\vec{x} = (\alpha^1, \dots, \vec{\theta}_1, \dots)$ are the total parameter setting. Such a concatenation corresponds to the hybrid tensor network in Fig. 8 (a). To find the ground state of Hamiltonian H , we can obtain the energy as

$$E(\vec{x}) = \frac{\langle \psi(\vec{x}) | H | \psi(\vec{x}) \rangle}{\langle \psi(\vec{x}) | \psi(\vec{x}) \rangle} = \frac{\sum_{i,j} \bar{\alpha}^i \alpha^j \langle \psi^i(\vec{\theta}_i) | H | \psi^j(\vec{\theta}_j) \rangle}{\sum_{i,j} \bar{\alpha}^i \alpha^j \langle \psi^i(\vec{\theta}_i) | \psi^j(\vec{\theta}_j) \rangle}, \quad (\text{B2})$$

and a minimization over the parameter space could lead to the solution.

We can see that such a hybrid tensor network contains the subspace expansion method as a special case. In particular, suppose we fix the parameters of the quantum tensors $|\psi^i(\vec{\theta}_i)\rangle$ and denote $|\psi^i(\vec{\theta}_i)\rangle = |\psi^i(\vec{\theta})\rangle$, then we can analytically solve the minimization of $E(\vec{x})$ as follows. Denote

$$H^{i,j} = \langle \psi^i(\vec{\theta}) | H | \psi^j(\vec{\theta}) \rangle, \quad S^{i,j} = \langle \psi^i(\vec{\theta}) | \psi^j(\vec{\theta}) \rangle. \quad (\text{B3})$$

Suppose we consider the subspace with $\langle \psi(\vec{x}) | \psi(\vec{x}) \rangle = 1$, then it is equivalent to optimize $E(\vec{x}) = \langle \psi(\vec{x}) | H | \psi(\vec{x}) \rangle$, or the function $E'(\vec{x}) = E(\vec{x}) - \lambda \langle \psi(\vec{x}) | \psi(\vec{x}) \rangle$ with a Lagrangian multiplier λ . Variation of of the new function $E'(\vec{x})$ gives

$$\delta E'(\vec{x}) = \sum_{i,j} (\alpha^j \delta \bar{\alpha}^i + \bar{\alpha}^i \delta \alpha^j) H^{i,j} - \lambda \sum_{i,j} (\alpha^j \delta \bar{\alpha}^i + \bar{\alpha}^i \delta \alpha^j) S^{i,j}, \quad (\text{B4})$$

and a local minimum solution requires $\delta E'(\vec{x}) = 0$, which is equivalent to

$$H^{i,j} \alpha^j = \lambda S^{i,j} \bar{\alpha}^i. \quad (\text{B5})$$

Writing the equation in the matrix form, it is equivalent to

$$H \vec{\alpha} = \lambda S \vec{\alpha}, \quad (\text{B6})$$

which coincides with the subspace expansion method.

In practice, we can optimize all the parameters in both quantum and classical tensors. We can simultaneously optimize them by treating $E(\vec{x})$ as a black box cost function. Alternatively, we can first optimize the parameters of the quantum tensor and then fix them and directly solve the optimal parameters of the classical tensor. Since the parameters are not simultaneously optimized, we may need to repeat the procedure several times until observing energy convergence.

b. Virtual qubits via classical tensors

In addition to extending the power of the quantum ansatz, we can also use the classical tensor to represent physical quantum systems, similar to classical tensor network. As shown in Fig. 8(b), we connect a rank- $(n+1)$ quantum tensor to a rank $d+1$ classical tensor network to represent a system of $n+d$ qubits. Here we assume the classical tensor network consists of low-rank classical tensors and admits efficient contraction, such as the matrix product state (MPS) as defined in Eq. (A2). In the remainder of the Appendix, we consider MPS as an example of the classical tensor network. Note that the discussion applies to general contractable classical tensor networks, such as tree tensor networks and the multi-scale entanglement renormalization ansatz (MERA).

Suppose the rank- $(n+1)$ quantum tensor ψ^{\dots} represents a set of n -qubit quantum states $\{|\psi^{i_1}\rangle\}$ and the classical tensor is given by $\alpha^{i_1, j_{n+1}, \dots, j_{n+d}} = \text{Tr}[\alpha_1^{i_1, j_{n+1}} \alpha_2^{j_{n+2}} \dots \alpha_n^{j_{n+d}}]$, then the hybrid tensor of Fig. 8(b) represents a quantum state

$$|\tilde{\psi}\rangle = \sum_{i_1, j_1, \dots, j_{n+d}} \alpha^{i_1, j_{n+1}, \dots, j_{n+d}} |\psi^{i_1}\rangle |j_{n+1}\rangle \dots |j_{n+d}\rangle. \quad (\text{B7})$$

For any tensor products of local observables $M = O_1 \otimes \dots \otimes O_{n+d}$, we have

$$\langle \tilde{\psi} | M | \tilde{\psi} \rangle = \sum_{i_1, i_1'} \langle \psi^{i_1'} | O_1 \otimes \dots \otimes O_n | \psi^{i_1} \rangle M^{i_1', i_1}, \quad (\text{B8})$$

with

$$M^{i'_1, i_1} = \sum_{j'_{n+1}, \dots, j'_{n+d}, j_{n+1}, \dots, j_{n+d}} \bar{\alpha}^{i'_1, j'_{n+1}, \dots, j'_{n+d}} \alpha^{i_1, j_{n+1}, \dots, j_{n+d}} \langle j'_{n+1} | O_{n+1} | j_{n+1} \rangle \dots \langle j'_{n+d} | O_{n+d} | j_{n+d} \rangle. \quad (\text{B9})$$

Here each $\langle \psi^{i'_1} | O_1 \otimes \dots \otimes O_n | \psi^{i_1} \rangle$ is obtained with a quantum computer and each element $M^{i'_1, i_1}$ is obtained by an efficient tensor contraction of the MPS ansatz. Note that the dimension of i_1 can be chosen as a small number similar to how we decide the bond dimension of the MPS ansatz. The definition also holds when the quantum tensor is an $(n+1)$ -partite state, where we can assign multiple qubits to the system that the i_1 label represents.

c. Local quantum correlation and non-local classical correlation

We can also use quantum tensors to represent quantum correlations of local subsystems and classical tensors to represent correlations between the subsystems. For example, consider two subsystems A and B with Hamiltonian $H = H_A + H_B + \lambda h_A \otimes h_B$ and a small coupling constant λ . We can use the hybrid tensor network in Fig. 8(c) to represent its ground state,

$$|\tilde{\psi}\rangle_{AB} = \sum_{i_1, i_2} \alpha^{i_1, i_2} |\psi^{i_1}\rangle_A \otimes |\psi^{i_2}\rangle_B. \quad (\text{B10})$$

Here $|\psi^{i_1}\rangle_A$ and $|\psi^{i_2}\rangle_B$ represent the state of subsystem A and B , respectively, and $\alpha^{i,j}$ is the classical tensor representing the correlation between A and B . If the quantum correlation is not too strong, we can set the rank of $\alpha_{i,j}$ to be a small number. The average energy of the Hamiltonian is

$$E = \frac{\langle \tilde{\psi} | H | \tilde{\psi} \rangle_{AB}}{\langle \tilde{\psi} | \tilde{\psi} \rangle_{AB}} = \frac{\sum_{i_1, i_2, i'_1, i'_2} \bar{\alpha}^{i'_1, i'_2} \alpha^{i_1, i_2} \left(H_A^{i'_1, i_1} S_B^{i'_2, i_2} + S_A^{i'_1, i_1} H_B^{i'_2, i_2} + \lambda h_A^{i'_1, i_1} h_B^{i'_2, i_2} \right)}{\sum_{i_1, i_2, i'_1, i'_2} \bar{\alpha}^{i'_1, i'_2} \alpha^{i_1, i_2} S_A^{i'_1, i_1} S_B^{i'_2, i_2}}, \quad (\text{B11})$$

where the matrices $H_A^{i'_1, i_1}$, $S_B^{i'_2, i_2}$, $S_A^{i'_1, i_1}$, $H_B^{i'_2, i_2}$, $h_A^{i'_1, i_1}$, $h_B^{i'_2, i_2}$ are defined in a general way as in Eq. (B3), that is, $M_{A(B)}^{i,j} = \langle \psi^i | M | \psi^j \rangle_{A(B)}$. Then we can get the Hamiltonian by measuring the matrices with a quantum computer and contract the classical tensors classically. Suppose each system A and B consists of n qubits so that the total system size is $2n$ qubits. We note that the energy terms can be obtained by only manipulating states of n qubits instead of $2n$ qubits.

In a similar way, we can extend the hybrid tensor network for two subsystems to k subsystems, as shown in Fig. 8(d). We use the matrix product state $\alpha^{i_1, i_2, \dots, i_k} = \text{Tr}[\alpha_1^{i_1} \alpha_2^{i_2} \dots \alpha_k^{i_k}]$ as the description of the correlation between subsystems. Suppose each subsystem is represented by quantum states $\{|\psi^{i_s}\rangle_s\}$, the hybrid tensor network of Fig. 8(d) represents a quantum state

$$|\tilde{\psi}\rangle_{AB} = \sum_{i_1, i_2, \dots, i_k} \alpha^{i_1, i_2, \dots, i_k} |\psi^{i_1}\rangle_1 \otimes |\psi^{i_2}\rangle_2 \dots \otimes |\psi^{i_k}\rangle_k. \quad (\text{B12})$$

To measure the expectation value of $M = O_1 \otimes \dots \otimes O_k$ with each O_s representing local observable on the s -th subsystem, we have

$$\langle \tilde{\psi} | M | \tilde{\psi} \rangle = \sum_{i_1, \dots, i_k, i'_1, \dots, i'_k} \bar{\alpha}^{i'_1, \dots, i'_k} \alpha^{i_1, \dots, i_k} M_1^{i'_1, i_1} \dots M_k^{i'_k, i_k}, \quad (\text{B13})$$

with

$$M_s^{i'_s, i_s} = \langle \psi^{i'_s} | O_s | \psi^{i_s} \rangle_s. \quad (\text{B14})$$

As a result, we can just use an n -qubit system to represent a kn -qubit system, and the bipartite version corresponds to $k=2$. The dimension of each index i_1, \dots, i_k should be a small number similar to the bond dimension of MPS. This is a general form of the hybrid quantum-MPS tensor network, and one can also consider other classical tensor networks, such as MERA. Note that here indices involved in the contraction between the quantum and classical tensors are both classical ones. Alternatively, one can also make a hybrid contraction, where the index of the quantum tensor is a quantum one, as shown in Eq. (A8).

Here the quantum tensors are used to represent the local n -qubit correlation, and the classical rank- k tensor is for the global correlation among these k clusters of qubits. Consequently, this kind of quantum-classical ansatz is suitable for systems where local correlation dominates over global correlation, such as the weak coupling of k qubit chains.

d. Non-local quantum correlation and local classical correlation

Instead of using the quantum processor to represent local correlations, one can also consider the classical-quantum two-depth tree structure in Fig. 8(e), where the classical tensors are used to represent local correlations of each subsystem, and the quantum tensor is used for representing the non-local correlation between the subsystems.

The idea is that, after we apply the quantum circuit to prepare a k -qubit state $|\psi\rangle$, we further connect a classical tensor network to each qubit to transform it to n qubits. Suppose we use the MPS for representing each subsystem as $\alpha^{i_s, \vec{j}_1 \dots \vec{j}_n} = \text{Tr}[\alpha_1^{i_s, \vec{j}_1^s} \dots \alpha_k^{j_n^s}]$, the state corresponding to Fig. 8(e) is

$$|\tilde{\psi}\rangle = \sum_{\vec{i}, \vec{j}^1, \dots, \vec{j}^k} \alpha^{i_1, \vec{j}^1} \dots \alpha^{i_k, \vec{j}^k} \psi_{i_1, \dots, i_k} |\vec{j}^1\rangle \otimes \dots \otimes |\vec{j}^k\rangle, \quad (\text{B15})$$

where we denote $\vec{i} = (i_1, \dots, i_k)$, $\vec{j}^s = (j_1^s, \dots, j_n^s)$, and $\psi_{i_1, \dots, i_k} = \langle \vec{i} | \psi \rangle$. To measure $M = O_1 \otimes \dots \otimes O_k$ with each O_s representing tensor products of local observables, we have

$$\langle \tilde{\psi} | M | \tilde{\psi} \rangle = \langle \psi | \tilde{O}_1 \otimes \dots \otimes \tilde{O}_k | \psi \rangle, \quad (\text{B16})$$

with each observable \tilde{O}_s obtained by classical tensor contraction as

$$\tilde{O}_s^{i'_s, i_s} = \sum_{\vec{j}^{s'}, \vec{j}^s} \tilde{\alpha}^{i'_s, \vec{j}^{s'}} \alpha^{i_s, \vec{j}^s} O_s^{\vec{j}^{s'}, \vec{j}^s}. \quad (\text{B17})$$

Again we only use k qubits to represent a system of nk qubits. Note that each subsystem may have a different number of qubits, and we can use multiple qubits to represent each index i_s to increase the bond dimension. When $n \gg 1$, this kind of hybrid tensor network can represent long-range correlation due to the effect of quantum tensor, and it may be applied to an exotic topological state. When n is a small number, it also represents a normalization of local correlations with classical ansatz.

e. Local and non-local quantum correlations

In the previous two cases, we use the classical tensor network to represent either local or non-local correlation and the quantum tensor to represent the other part. Here we show how to use the quantum tensor to represent both the local and non-local correlations. Considering a two-depth tree structure of Fig. 8(f), it represents a state

$$|\tilde{\psi}\rangle = \sum_{i_1, \dots, i_k} \psi_{i_1, \dots, i_k} |\psi_1^{i_1}\rangle \dots |\psi_k^{i_k}\rangle, \quad (\text{B18})$$

where $\psi_{i_1, \dots, i_k} = \langle i_1 | \dots \langle i_k | \psi \rangle$ denotes the quantum tensor of the correlation between the subsystems and $\{|\psi_s^{i_s}\rangle\}$ denotes the quantum states for each subsystem s . Similar to the previous cases, we can measure the expectation values of local observables. To measure $M = O_1 \otimes \dots \otimes O_k$ with each O_s representing tensor products of local observables on subsystem s , we have

$$\langle \tilde{\psi} | M | \tilde{\psi} \rangle = \langle \psi | \tilde{O}_1 \otimes \dots \otimes \tilde{O}_k | \psi \rangle, \quad (\text{B19})$$

with each observable \tilde{O}_s being

$$\tilde{O}_s^{i'_s, i_s} = \langle \psi_s^{i'_s} | O_s | \psi_s^{i_s} \rangle \quad (\text{B20})$$

obtained via the method discussed in Sec. A3. Here we represent a system of nk qubits by controlling a quantum device with up to $\max\{n, k\}$ qubits. We can also use multiple qubits for each index i_s to increase the bond dimension. Suppose the quantum states are generated as $|\psi\rangle = U |0\rangle_0^{\otimes k}$ and $|\psi_s^{i_s}\rangle = U_s |i_s\rangle_s |0\rangle_s^{\otimes(n-1)}$, the hybrid tensor network of Fig. 8(f) can be obtained via a quantum circuit

$$|\tilde{\psi}\rangle = U_k \left(\dots U_2 \left(U_1 \left(U |0\rangle_0^{\otimes k} \otimes |0\rangle_1^{\otimes(n-1)} \right) \otimes |0\rangle_2^{\otimes(n-1)} \right) \dots \otimes |0\rangle_k^{\otimes(n-1)} \right), \quad (\text{B21})$$

where each U_s applies to the s th qubit of the first k qubits with subscript 0 and the new $n-1$ qubits with subscript s . While such a quantum circuit requires to jointly control nk qubits, our hybrid tensor network allows us to represent the same state by controlling up to $\max\{n, k\}$ qubits.

2. Cost for a general hybrid tree tensor network

Now we give a resource estimation for the cost of calculating expectation values of tensor products of local observables on a hybrid tree tensor network.

Starting from a chosen node referred to as root in a tree, we separate other vertices into different layers according to the distance to the root. For each node, it can be either a classical tensor network or a quantum tensor. In order to efficiently contract the whole tensor network, we only consider classical tensor networks that can be efficiently contracted, for instance, matrix product states (MPS). Suppose the tree has a maximal of D layers, and each node has at most t connected, it corresponds to a tree with depth D and maximal degree t , and we call a (D, t) -tree. The total number of nodes is upper bounded by $\mathcal{O}(t^{D-1})$, which is a polynomial function of t with a constant D and $t \geq 1$.

Now suppose we aim to measure the expectation value of tensor products of local observables. For each node with degree t , we denote the cost to be C_q or C_c for a quantum or a classical tensor, respectively. In the i th layer, denote n_i^q and n_i^c to be the numbers of quantum and classical tensors, respectively, which satisfy $n_i^q + n_i^c \leq t^{i-1}$. The cost of contracting the i th layer is thus $C_i = C_q n_i^q + C_c n_i^c \leq t^{i-1}(C_q + C_c)$ and the total cost of contracting the whole tree is $\mathcal{O}(t^{D-1})$ when $t \geq 1$ and $D = \mathcal{O}(1)$. Note that the number of qubits N represented by the (D, t) -hybrid tree tensor network is $N = \mathcal{O}(t^{D-1})$, so the cost is also linear to the number of qubits. We summarize the result as follows.

Proposition 1. *The cost for evaluating the expectation values of local observables of a (D, t) -hybrid tree tensor network is at most $\mathcal{O}(t^{D-1}(C_q + C_c))$ or $\mathcal{O}(N(C_q + C_c))$. Here $N = \mathcal{O}(t^{D-1})$ is the number of qubits represented by the (D, t) -hybrid tree tensor network.*

The value of C_q depends on the bond dimension of the connection between two nodes and the number of samples required for suppressing shot noise to a desired accuracy ε . The value of C_c depends on the choice of the classical tensor network and the bond dimension as well. Suppose the bond dimension of each contracted index is upper bounded by χ , then we have $C_q = \mathcal{O}(\chi^2/\varepsilon^2)$ and $C_c = \mathcal{O}(t\chi^4)$ for MPS. Therefore, we have

Proposition 2. *Consider a (D, t) -hybrid tree tensor network with quantum tensors and classical MPS tensor networks with bond dimension χ . The cost evaluating the expectation values of local observables is at most $\mathcal{O}(t^{D-1}(\chi^2/\varepsilon^2 + t\chi^4))$ or $\mathcal{O}(N(\chi^2/\varepsilon^2 + t\chi^4))$.*

Note that here we regard the cost of classical and quantum tensor contractions to be the same and add them together to be the total cost. In practice, classical and quantum computation are independently run on a classical and a quantum processor, so they are totally parallel. If we only focus on the resource cost for the quantum processor, the cost scales as $\mathcal{O}(N(\chi^2/\varepsilon^2))$, which is linear to the number of qubits and polynomial to the bond dimension and inverse polynomial to the simulation accuracy.

3. Entanglement and correlation of hybrid tensor network

In this section, we discuss the entanglement and correlation properties of the hybrid tree tensor network. We consider a tree structure with two layers and three cases with local or non-local correlations being either classical or quantum. The discussion can be generalized to trees with multiple layers.

a. Local quantum correlation and non-local classical correlation

First, we focus on the hybrid tensor network with local quantum correlation and non-local classical correlation introduced in Sec. B 1 c. Here we take the classical tensor as MPS for an illustration. As shown in Fig. 9(a), we separate the whole kn qubits into two subsystems with a blue boundary line and denote the left and the right parts to be A and \bar{A} , respectively. Without loss of generality, we choose two kinds of boundaries — one is in the bulk of the classical tensor at the first layer, where the boundary is between indices i_l and i_{l+1} (in the same time between j_n of $\Psi_j^{i_l}$ and j_1 from $\Psi_j^{i_{l+1}}$); the other is in the bulk of the quantum tensor at the second layer, where the boundary is between indices $j_{l'}$ and $j_{l'+1}$.

For the first kind of bipartition between i_l and i_{l+1} , the entanglement of the subsystem is upper bounded by the bond dimension of the index s_l of the MPS, which is normally a constant number that is independent of the subsystem size. As a result, the correlation between these n -qubit clusters is weak. The second kind of bipartition between $j_{l'}$ and $j_{l'+1}$ is inside the quantum tensor $\Psi_j^{i_l}$, which is represented by a general quantum state. Thus the entanglement entropy can be in principle proportional to $\min\{l', n - l'\}$, which is proportional to the subsystem size of the quantum tensor.

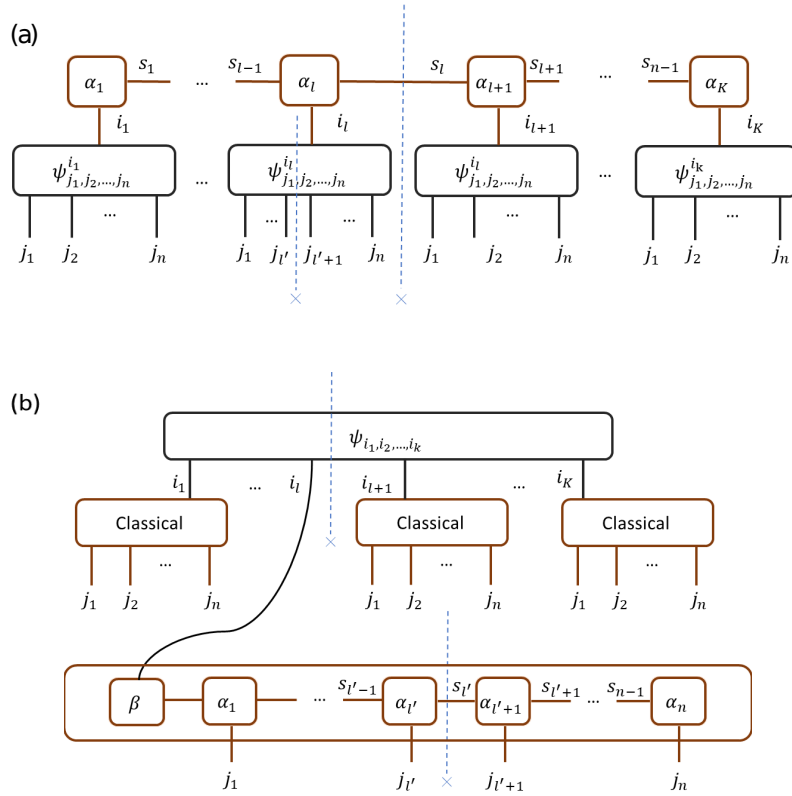


FIG. 9. Illustration of the hybrid tensor network with bipartitions: (a) quantum-classical ansatz with the classical tensor being a MPS introduced in Sec. B 1 c; (b) classical-quantum ansatz introduced in Sec. B 1 d. Here we separate the whole Kn -qubit system into two parts, that is, the left and the right subsystems, and the boundary is denoted by the dotted blue line. Without loss of generality, we choose two kinds of boundaries: one is in the bulk of the (classical or quantum) tensor at the first level, where the boundary is between indices i_l and i_{l+1} ; the other is in the bulk of the tensor at the second level, where the boundary is between indices $j_{l'}$ and $j_{l'+1}$.

The previous analyses on entanglement can also be revealed by the correlation functions. If we select two local observables O_1 and O_2 inside the bulk of any local quantum tensors, the correlation function $\langle O_1 O_2 \rangle$ could be even a constant. However, if they are located in different local quantum tensors, the correlation suffers an exponential decay $\langle O_1 O_2 \rangle \sim \exp(-a|l_2 - l_1|)$, where a is some constant depending on the chosen MPS and $|l_2 - l_1|$ labels the distance between the two quantum tensors where O_1 and O_2 are inside. As shown in Fig. 10, this scaling can be obtained by first contracting the local observables O_1 and O_2 with the quantum tensors, and then the total result becomes two new observables say M_1 and M_2 in the MPS tensor network.

b. Local classical correlation and non-local quantum correlation

Next, we study the hybrid tensor network introduced in Sec. B 1 d, where one has local classical correlation and non-local quantum correlation. As shown in Fig. 9 (b), the whole kn -qubit is separated into two parts by the blue boundary. We also choose two kinds of boundaries — one is in the bulk of the quantum tensor between indices i_l and i_{l+1} ; the other is in the bulk of the classical tensor between indices $j_{l'}$ and $j_{l'+1}$.

For the bipartition between i_l and i_{l+1} inside the global quantum tensor $\psi_{i_1, i_2, \dots, i_k}$, the entanglement can be proportional to $\min\{l, k - l\}$, with the subsystem size being $|A| = nl$ and $|\bar{A}| = n(k - l)$. As a result, when $k \gg 1$ and $n = \mathcal{O}(1)$, the hybrid tensor network can have a volume law entanglement scaling due to the contribution from the quantum tensor. For the regime $n \sim k$, the entanglement is weaker but still stronger than the area law. From this point of view, the hybrid tree tensor network could represent more complicated entanglement than pure classical tensor networks. For the second kind of bipartition between $j_{l'}$ and $j_{l'+1}$, the entanglement of the subsystem is upper bounded by the bond dimension of the index $s_{l'}$ of the local MPS, which is normally a constant number independent of the subsystem dimension. As a result, the correlations inside these n -qubit clusters are weak.

Similarly, the previous analyses on entanglement can be revealed by the correlation function. If two local observables

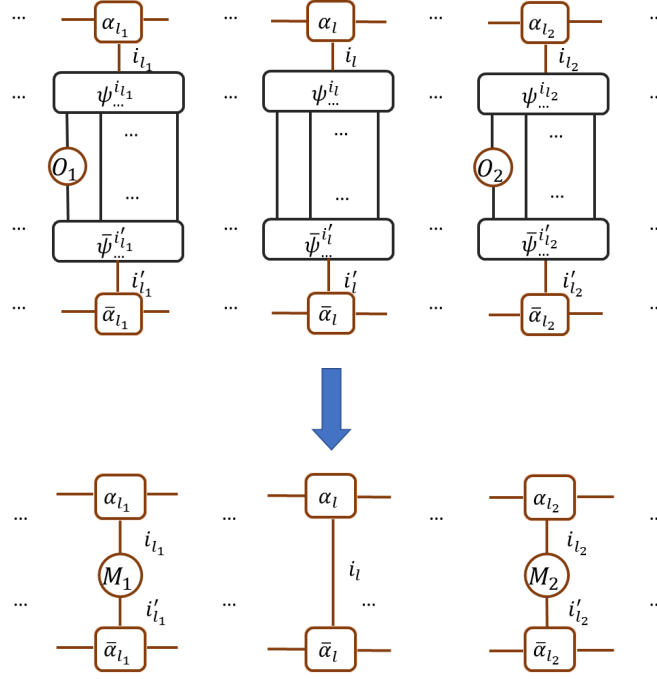


FIG. 10. The contraction process to extract the correlation function of the quantum-classical hybrid tensor network introduced in B 1 c. Here the classical ansatz is an MPS. The two observables O_1 and O_2 are in two local quantum tensors $\Psi^{i_{l_1}}$ and $\Psi^{i_{l_2}}$, respectively, with i_{l_1} and i_{l_2} are two classical indices. Similar to the extraction of expectation value in Fig. 7 (a), We first contract O_1 and O_2 with the local quantum tensors to get two new observables M_1 and M_2 for the classical MPS. Here we assume that $\langle \Psi^{i'_l} | \Psi^{i_l} \rangle = \delta_{\{i_l i'_l\}}$ for simplicity, that is, the quantum states indexed by i_l are orthogonal to each other. In this way, the contraction result is the identity for other quantum tensors which do not contain O_1 or O_2 . As a result, the correlation function shows $\langle O_1 O_2 \rangle = \langle M_1 M_2 \rangle_{\{MPS\}}$, where the second expectation value is on the MPS and shows an exponential decay.

O_1 and O_2 are inside the bulk of any local classical tensor, the correlation function $\langle O_1 O_2 \rangle$ decays exponentially. However, if they are located in different local classical tensors, the correlation could be some constant or decay polynomially. One can first contract the local observables O_1 and O_2 with the classical tensors, and then the total result becomes two new observables for the general quantum tensor.

c. Local quantum correlation and non-local quantum correlation

At last, we consider the hybrid tensor network introduced in Sec. B 1 e, where both local and non-local correlations are represented by quantum tensors. As a result, it can possess a strong correlation both for local and global correlation. The entanglement entropy and correlation function can be analyzed in the same way above.

For the general hybrid tree structure, the analyses are also similar. For the entanglement, one just needs to check the boundary is in the bulk of quantum or classical tensor. For the correlation function, one can obtain its behavior by iterative contractions and check whether the final new observables are in a quantum or classical tensor.

Appendix C: Numerical simulation

Here we discuss the details of numerical simulation for finding the ground state of 1D and 2D spin systems. We review the framework of imaginary time evolution and discuss how to implement it with hybrid tensor networks.

We first briefly review the variational quantum simulation algorithm of imaginary time evolution. We consider Hamiltonian $H = \sum_i \lambda_i h_i$ with coefficients λ_i and tensor products of Pauli matrices h_i . The normalized state at imaginary time τ is $|\psi(\tau)\rangle = \frac{e^{-H\tau}|\psi(0)\rangle}{\sqrt{\langle \psi(0) | e^{-2H\tau} | \psi(0) \rangle}}$ and the Wick-rotated Schrödinger equation is

$$\frac{d|\psi(\tau)\rangle}{d\tau} = -(H - E_\tau) |\psi(\tau)\rangle \quad (\text{C1})$$

where $E_\tau = \langle \psi(\tau) | H | \psi(\tau) \rangle$ is the expected energy at imaginary time τ . The ground state can be determined from the long time limit of the Wick-rotated Schrödinger equation $|\psi\rangle_{\text{GS}} = \lim_{\tau \rightarrow \infty} |\psi(\tau)\rangle$. Consider a normalized trial state $|\psi(\vec{x}(\tau))\rangle$ with real parameters \vec{x} , the imaginary time evolution of the Schrödinger equation on the trial state space is

$$\sum_i \frac{\partial |\psi(\vec{x}(\tau))\rangle}{\partial \theta_i} \dot{\theta}_i = -(H - E_\tau) |\psi(\vec{x}(\tau))\rangle. \quad (\text{C2})$$

Applying the McLachlans variational principle, which minimizes the distance between the evolution of trial state $\frac{\partial |\psi(\vec{\theta}(\tau))\rangle}{\partial t}$ and $-iH |\psi(\vec{\theta}(\tau))\rangle$, we have

$$\delta \| (d/d\tau + H - E_\tau) |\psi(\vec{x}(\tau))\rangle \| = 0, \quad (\text{C3})$$

which determines the evolution of the parameters

$$\sum_j A_{i,j} \dot{\theta}_j = -C_i, \quad (\text{C4})$$

with the matrix elements of A and C given by

$$A_{i,j} = \Re \left(\frac{\partial \langle \psi(\vec{\theta}(t)) |}{\partial \theta_i} \frac{\partial |\psi(\vec{\theta}(t))\rangle}{\partial \theta_j} \right), \quad C_i = \Re \left(\frac{\partial \langle \psi(\vec{\theta}(t)) |}{\partial \theta_i} H |\psi(\vec{\theta}(t))\rangle \right). \quad (\text{C5})$$

Therefore, we can effectively simulate imaginary time evolution by tracking the evolution of the parameters.

To variationally simulate imaginary time evolution, we have to be able to calculate A and C for any given parameters. When $|\psi(\vec{x})\rangle$ is directly prepared by a quantum circuit, we can obtain the matrix elements by a modified quantum circuit by introducing an ancillary qubit [11, 28]. When we consider trial states represented by a hybrid tensor network, we can calculate A and C by making use of a similar method for calculating the expectation values of hybrid tensor networks. The main idea is to generalize the circuit to implement the contraction of two quantum tensors. We leave the circuit implementation of the matrix elements and the application of the hybrid tensor network in simulating real-time dynamics to future work.

In this work, we calculate the matrix elements by the finite difference method. For example, to calculate each $A_{i,j}$, we can approximate it as

$$\begin{aligned} A_{i,j} &= \Re \left(\frac{(\langle \psi(\vec{\theta} + \delta\theta_i) | - \langle \psi(\vec{\theta}) |) (|\psi(\vec{\theta} + \delta\theta_j)\rangle - |\psi(\vec{\theta})\rangle)}{\delta\theta_i \delta\theta_j} \right), \\ &= \frac{1}{\delta\theta_i \delta\theta_j} \Re \left(\langle \psi(\vec{\theta} + \delta\theta_i) | \psi(\vec{\theta} + \delta\theta_j) \rangle - \langle \psi(\vec{\theta}) | \psi(\vec{\theta} + \delta\theta_j) \rangle - \langle \psi(\vec{\theta} + \delta\theta_i) | \psi(\vec{\theta}) \rangle + \langle \psi(\vec{\theta}) | \psi(\vec{\theta}) \rangle \right). \end{aligned} \quad (\text{C6})$$

Here the first and the last terms correspond to the normalization of the hybrid tensor, which is 1 for the hybrid TTN considered in the simulation. The second two terms are overlap with two different hybrid tensor networks. Again, calculating such overlaps requires quantum circuits similar to calculating expectation values. In our simulation, for simplicity, we obtain the overlaps by directly contracting the quantum tensors by summing over the state vector array. For each C_i element, it can be obtained via the difference of the energy gradient,

$$C_i = \frac{\langle \psi(\vec{\theta} + \delta\theta_i) | H | \psi(\vec{\theta} + \delta\theta_i) \rangle - \langle \psi(\vec{\theta}) | H | \psi(\vec{\theta}) \rangle}{\delta\theta_i}. \quad (\text{C7})$$

Therefore, the C vector can be obtained from the finite difference of energy changes.

Appendix D: Applications

In this section, we discuss potential applications of the hybrid tensor network in practical problems in chemistry, condensed matter physics, quantum field theory, and quantum gravity thought experiments.

1. Chemistry

We first focus on the application in chemistry for solving the molecular vibronic spectra. The vibrational and electronic structure of a molecule generally assumes the Born-Oppenheimer approximation by treating the electrons and nuclei separately. Here we show how to go beyond the Born-Oppenheimer with the hybrid tensor network method. Consider the molecular Hamiltonian in atomic units as

$$H_{\text{mol}} = - \sum_i \frac{\nabla_i^2}{2} - \sum_I \frac{\nabla_I^2}{2M_I} - \sum_{i,I} \frac{Z_I}{|\mathbf{r}_i - \mathbf{R}_I|} + \frac{1}{2} \sum_{i \neq j} \frac{1}{|\mathbf{r}_i - \mathbf{r}_j|} + \frac{1}{2} \sum_{I \neq J} \frac{Z_I Z_J}{|\mathbf{R}_I - \mathbf{R}_J|}. \quad (\text{D1})$$

with M_I , \mathbf{R}_I , and Z_I being the mass, position, and charge of nuclei I , respectively, and \mathbf{r}_i being the position of electron i . Given the location of the nucleus, the electronic Hamiltonian is

$$H_e(\mathbf{R}_I) = - \sum_i \frac{\nabla_i^2}{2} + \sum_{i,I} \frac{Z_I}{|\mathbf{r}_i - \mathbf{R}_I|} + \frac{1}{2} \sum_{i \neq j} \frac{1}{|\mathbf{r}_i - \mathbf{r}_j|}, \quad (\text{D2})$$

and the total Hamiltonian can be represented as

$$H_{\text{mol}} = - \sum_I \frac{\nabla_I^2}{2M_I} + \frac{1}{2} \sum_{I \neq J} \frac{Z_I Z_J}{|\mathbf{R}_I - \mathbf{R}_J|} + H_e(\mathbf{R}_I). \quad (\text{D3})$$

Under the Born-Oppenheimer approximation, we assume the electrons and nuclei are in a product state,

$$|\psi\rangle = |\psi\rangle_n |\psi\rangle_e, \quad (\text{D4})$$

and the ground state energy under the Born-Oppenheimer approximation is solved by

$$E_0 = \min_{|\psi\rangle_n} \min_{|\psi\rangle_e} \langle \psi | \langle \psi | H_{\text{mol}} | \psi \rangle_n | \psi \rangle_e. \quad (\text{D5})$$

Because only the electronic Hamiltonian $H_e(\mathbf{R}_I)$ depends on electronic state $|\psi\rangle_e$, the minimisation over the electronic state $|\psi\rangle_e$ is equivalent to finding the ground state of the electronic Hamiltonian $H_e(\mathbf{R}_I)$. Suppose we solve the electronic structure for any $H_e(\mathbf{R}_I)$ by finding

$$V_0^e(\mathbf{R}_I) = \min_{|\psi\rangle_e} \langle \psi | H_e(\mathbf{R}_I) | \psi \rangle_e, \quad (\text{D6})$$

then the ground state of H_{mol} can be found by solving the ground state of H_0 ,

$$H_0 = - \sum_I \frac{\nabla_I^2}{2M_I} + \frac{1}{2} \sum_{I \neq J} \frac{Z_I Z_J}{|\mathbf{R}_I - \mathbf{R}_J|} + V_0^e(\mathbf{R}_I). \quad (\text{D7})$$

The Born-Oppenheimer approximation enables us to solve the molecular Hamiltonian by separately solving the electronic Hamiltonian and the nuclei Hamiltonian. We thus only need to operate a quantum system either for the electronic Hamiltonian or the nuclei Hamiltonian.

The conventional approach to go beyond the Born-Oppenheimer approximation is to consider the electrons and nuclei together as a whole system and directly solve the Hamiltonian H_{mol} . However, this requires to store the joint entangled state of electrons and nuclei, making it harder to simulate with near-term quantum computers. Since the nuclei is much heavier than the electrons, even though the Born-Oppenheimer approximation breaks, the entanglement between electrons and nuclei may still be small. Therefore, we can use the hybrid tree tensor network to represent the whole state. Suppose the ansatz for the electrons and nuclei are $\{|\psi_e^i(\vec{\theta}_e)\rangle\}$ and $\{|\phi_n^i(\vec{\theta}_n)\rangle\}$, respectively. Then a hybrid tensor network representation of the joint state is

$$|\tilde{\psi}\rangle = \sum_i \alpha_i |\psi_e^i(\vec{\theta}_e)\rangle |\phi_n^i(\vec{\theta}_n)\rangle, \quad (\text{D8})$$

and we use it to represent the ground state of the molecule by only controlling states of either the electrons or the nuclei. We can also apply the hybrid tensor network for representing the electrons or the nuclei to further reduce the size of the quantum system we need to control.

2. Condensed matter physics

Many interesting quantum phenomena could be captured by the model of weakly- or medium-coupled subsystems, as the models we considered in Fig. 5(a) in the main context. However, the interactions of local subsystems could generate complex multipartite entanglement and lead to effective quasi-particle transportation between the quantum systems, making it hard to simulate classically. In this section, we discuss the use of variational quantum simulation and the hybrid tensor network approach to search for Majorana zero-modes and the topological phase transition in correlated materials.

We first consider a spinless one-dimensional tight-binding spin chain representation of a p -wave superconductor introduced by Kitaev [41],

$$H = - \sum_{i=1}^{N-1} \left(t c_i^\dagger c_{i+1} + \Delta c_i c_{i+1} + h.c. \right) - \mu \sum_{i=1}^N n_i, \quad (\text{D9})$$

where t is the nearest-neighbor hopping amplitude, μ is the chemical potential, and $\Delta = |\Delta|e^{i\theta}$ is the induced superconducting gap. This toy model of p -wave superconductor is in contrast to standard s -wave pairing since it couples electrons with the same spin. When tuning the hopping amplitude and chemical potential to $|\Delta| = t > 0$, $\mu = 0$, unpaired Majorana fermions appear at the boundary of the chain, which results in a topologically non-trivial phase. Kitaev's quantum wire bridge proposal provides guidance for realizing the topological p -wave superconductors. In practice, this can be difficult to be physically realized because besides from the necessary condition for the unpaired Majorana, which requires an energy gap in the excitation spectrum, i.e., superconductivity in the bulk, the ground state of the connected chain has to be degenerate, where Majorana fermions still exist at the ends of the spin chain, and this is the parity condition.

When inducing the p -wave superconductivity, Zeeman coupling can also be proximity induced in the film by an adjacent magnetic insulator. Aside from the proximity induced p -wave superconductivity in the film of the topological insulator and s -wave superconductor, we can replace the magnetic insulator by other materials. Sau *et al.* [60] showed that tuning the Zeeman coupling of spins in the spin-orbit-coupled systems could also induce a topological phase transition, and for the Zeeman coupling above the critical value, there are localized Majorana zero-energy modes at the two ends of a semiconducting quantum nanowire. This provides a proposal for searching for the Majorana zero-energy modes in materials with strong spin-orbit coupling. The spinless toy model could not describe the conventional materials in which electrons have spin 1/2, and more importantly, electrons in correlated materials inherently have multiple degrees of freedom, which can be difficult to simulate. Nevertheless, we are able to use the variational quantum algorithms and our hybrid approach to determine the energy spectra of the bulk materials. For instance, we can store the degrees of freedom of electrons in the bulk materials with a quantum processor and also use the classical (quantum) tensor to represent the coupling effect. We are able to solve the ground state and low lying excited eigenstates of strongly correlated materials involving spinless fermions that hop along a certain translationally invariant one-dimensional spin chain or a general spin model with spin-orbit interactions. By tuning the coupling and bulk properties, such as spin-orbit coupling, chemical potential μ , external magnetic field, etc., we could drive the system to topologically non-trivial phase [39, 40, 42, 43]. As the boundary condition of the superconductor heterostructures is usually much simpler than the bulk, the tensor-network-type algorithms would be suitable to resolve this category of problems. The quantum simulation of the topological phase might be able to provide an avenue for the systematic search of topological superconductivity from heterostructures consisting of strongly correlated materials.

3. Quantum simulation of quantum field theories

Since we are interested in simulating systems with large degrees of freedom using the hybrid tensor network, a perfect physical application might be the quantum simulation of quantum field theories. If we wish to simulate the quantum field theory process, for instance, the scattering process in a collider physics setup, we could consider using the hybrid tensor network to simulate it in the near-term quantum device. For instance, one could consider using the setup of the Jordan-Lee-Preskill algorithm [44, 45], and try to use the hybrid tensor network to perform state preparation and time evolution. In particular, we could imagine split the whole system into small subsystems. For coupling constants and entanglement, both with an intermediate amount, our hybrid tensor network might be useful.

Now we make some more precise suggestions. Say that we are simulating a specific non-integrable, local, latticed-version of quantum field theory in a near-term quantum device, for instance, the $\lambda\phi^4$ theory in 1+1 dimension, with the Lagrangian density

$$\mathcal{L}(\phi) = \frac{1}{2} [\partial^\mu \phi \partial_\mu \phi - m^2 \phi^2] - \frac{\lambda}{4!} \phi^4. \quad (\text{D10})$$

Here ϕ is the scalar field where the whole local Hilbert space will be truncated, μ is the spacetime coordinate indices, m is the mass and λ is the coupling.

We could compute the initial states and the time evolution process using variational quantum simulation. Say that we are taking N sites in total. One could consider making a variational ansatz by dividing the whole system by two. A superposition of several product states will cover a large amount of the whole Hilbert space with bounded entanglement. One could deal with the system when the coupling is not weak, but also not super-strong using the above ansatz. The superposition coefficients might be treated quantumly, where the hybrid tensor network might play an important role. This is similar to the situation discussed in the numerical example we present in this paper. For instance, the ansatz could be naturally assigned when we are considering the time evolution of a two-particle scattering event

$$|\text{ansatz}\rangle = \sum_{\text{superposition}} |\text{left}\rangle \otimes |\text{right}\rangle, \quad (\text{D11})$$

where the left and right Hilbert spaces could be split naturally. Note that we should be careful about providing enough entanglement towards the superposition since quantum field theory itself provides fruitful vacuum entanglement.

One could provide another possibility where the hybrid tensor network might play an important role. Say that we wish to take a d -dimensional local Hilbert space in each site. One could consider the superposition of low energy states as the variational ansatz, where the high energy sector could be less excited. This corresponds to the hybrid tensor network of Fig. 8(f). This suggestion might be helpful for a system with strong coupling when the system is approaching a critical point that is scale-free.

4. Quantum simulation of quantum gravity thought experiments

Aside from the quantum simulation of quantum field theories, we could also consider using a hybrid tensor network to simulate quantum gravity thought experiments. There are, of course, many possible quantum simulation problems that are not solved by conventional methods. We will take a specific example here, the traversable wormhole.

How to make a wormhole traversable, which is typically not allowed in general relativity due to the energy condition? Recently people found a beautiful thought experiment as a solution to this problem with the help of quantum information theory and holography (see [50], and also [51, 61, 62]). This thought experiment is set in light of the dual descriptions between quantum entanglement and Einstein-Rosen bridge (ER=EPR) [63], where a thermofield double state in two conformal field theories (CFTs) is dual to a two-sided wormhole in the dual gravity theory. With a coupling between two boundary CFTs, one is allowed to send a gravitational shockwave [64] into the bulk with negative energy, which introduces the time advance instead of Shapiro time delay when the ingoing boundary signal is passing through the spacetime discontinuity of the shockwave, making the wormhole traversable.

This thought experiment could be interpreted as a modification of Hayden-Preskill protocol [46] for extracting quantum information dropping inside a black hole from Hawking radiation, but without introducing unknown Planckian physics to solve the no-cloning paradox where information is never duplicated in the bulk. It is also allowed for us to explore more physics about black hole interior with some concrete boundary theories assuming ER=EPR.

To introduce this formalism more concretely, we start from a simple classical, non-relativistic analog of the traversable wormhole, as illustrated by [51]. Imagine that there are two identical systems, L , and R , with no interaction initially. In both systems there are N particles with position $\bar{x}_i^{L(R)}$ and momentum $\bar{p}_i^{L(R)}$. At the time $t = 0$, they are set to have the same positions but opposite momenta,

$$\begin{aligned} \bar{x}_i^L(0) &= \bar{x}_i^R(0) , \\ \bar{p}_i^L(0) &= -\bar{p}_i^R(0) , \end{aligned} \quad (\text{D12})$$

to simulate a thermofield double state for two boundary CFTs. Now, we are considering adding a small perturbation $\delta x_\alpha^R(t_R)$ at the original trajectory $\bar{x}_\alpha^R(t_R)$ for $t_R < 0$ and a specific particle α . According to the perturbation, generically, the location of other particles will be affected, especially when the system is chaotic. Thus, we obtain a perturbation for another particle β , at time $t = 0$ in this system, $\delta x_\beta^R(0)$. Then we choose a coupling between L and R system at time $t = 0$, for simplicity, with the potential

$$V = \frac{1}{2} k_{\text{in}} (x_\beta^R - x_\beta^L)^2 , \quad (\text{D13})$$

where $x_i^{L(R)}$ denotes the quantities after the perturbation. After turning on this potential for a very small time interval g , it leads to a perturbation over the momentum of β in L , $\delta p_\beta^L(0^+)$, where 0^+ denotes a time slightly larger than

$t = 0$ which could be set as g . Now turn off the interaction and evolve the system L to a time scale t_L . Because of the perturbation of the momentum $\delta p_\beta^L(0^+)$ we get the perturbation of momentum for α in L at time t_L , $\delta p_\alpha^L(t_L)$. This formalism could be regarded as teleportation from the perturbation of location for a specific particle in the system R at time t_R , to the perturbation of momentum for the dual particle in the dual system L at time t_L . If the dependence between $\delta x_\alpha^R(t_R)$ and $\delta p_\alpha^L(t_L)$ is simple, and some features are universal for different initial conditions of the system, we might say that the teleportation is successful.

One can generalize this logic to the quantum information scenario [51]. Consider the thermofield double state of two identical quantum systems, L and R . Similarly, we set two times t_L and t_R , and we add a small interaction $V = O_L(0)O_R(0)$ between two systems. Namely, we add the following factor into the path integral when evaluating correlation functions

$$\exp(igV) = \exp(igO_L(0)O_R(0)) , \quad (\text{D14})$$

where g is a small number. Now consider an operator ϕ_R and its dual operator ϕ_L . Add a small unitary perturbation on ϕ_R at time t_R , $\exp(i\epsilon_R\phi_R(t_R))$, we measure ϕ_L at t_L as

$$\left\langle e^{-i\epsilon_R\phi_R(t_R)} e^{-igV} \phi_L(t_L) e^{igV} e^{i\epsilon_R\phi_R(t_R)} \right\rangle = \langle e^{-igV} \phi_L(t_L) e^{igV} \rangle - i\epsilon_R \langle [\phi_R(t_R), \phi_L(t_L)] \rangle_V + \mathcal{O}(\epsilon_R^2) , \quad (\text{D15})$$

where

$$\langle [\phi_R(t_R), \phi_L(t_L)] \rangle_V \equiv \langle [\phi_R(t_R), e^{-igV} \phi_L(t_L) e^{igV}] \rangle . \quad (\text{D16})$$

Thus, the non-vanishing value of $\langle [\phi_R(t_R), \phi_L(t_L)] \rangle_V$ shows that there are some messages that have been teleported from R to L . In the quantum system dual to the wormhole geometry, this quantity could measure the traversability of the wormhole, and the whole process has a clear geometric picture as introduced before. For explicit holographic models, for instance, the Sachdev-Ye-Kitaev (SYK) model [65], it is investigated in the very detail in [61].

It is known that an honest holographic model representing features of emergent gravity requires boundary systems to have a large number of degrees of freedom [66]. Thus, to construct quantum gravitational dynamics in the bulk, strong computational power is needed to simulate complicated boundary quantum dynamics, lightning possible opportunities for quantum simulation. About quantum simulation of traversable wormholes, until now, people mostly use analog quantum simulation in cold-atomic systems to study them (see, for instance, [67] or [68]). Works based on analog simulations are very important for many quantum-mechanical problems at large scale, especially for those who could obtain dynamical quantities with real physical meanings. However, the variational quantum simulation might also be suitable and important, and it has the following certain advantages. Firstly, variational quantum simulation has more degrees of freedom to operate in the near-term digital quantum computer instead of a cold-atomic device without universal gates. Secondly, it is hard to implement a strongly-coupled model with Majorana fermions and all-to-all interactions in a cold-atomic system, while a digital setup could easily overcome this problem with certain encoding protocols.

The hybrid tensor network will be specifically useful for traversable wormhole simulations for near-term quantum computing. For specific chaotic, holographic models, the algorithm will involve a state preparation of a thermofield double at a certain temperature, where the entanglement between two sides is around an intermediate scale. Since the coupling between the two systems is weak, we could use the hybrid tree tensor network, where the whole system is divided into two subsystems. We could use time-dependent variational quantum simulation with a hybrid tree tensor network using existing algorithms (for instance, see [11]) to compute correlation functions between two sides. We leave those interesting possibilities and actual simulation in future research.